Comparison of human versus mouse CYP1A1 and CYP1A2 TCDD-induced enzyme activities in liver

For BaP hydroxylase and EROD as two activities associated predominantly with CYP1A1, the correlations between enzyme activities (Fig. 3A) and mRNA levels (Fig. 1A) are extremely variable for BaP hydroxylase but quite consistent for EROD activity. Thus, B6 mice exhibit one-half as much TCDD-induced BaP hydroxylase activity (per unit of mCYP1A1 mRNA) as *uPA/SCID* mice (Table 2). The B6 mouse shows ~170 times more induced BaP hydroxylase activity (per unit of mCYP1A1 mRNA), compared with the *hCYP1A1_1A2_Cyp1a1/1a2(−/−)* mouse's induced BaP hydroxylase activity (per unit of hCYP1A1 mRNA). Chimeric mice exhibit ~6.2-fold more induced BaP hydroxylase activity (per unit of hCYP1A1 mRNA) than *hCYP1A1_1A2_Cyp1a1/1a2(−/−)* mice (Table 2). The *uPA/SCID* mouse shows ~42 times more induced BaP hydroxylase activity (per unit of mCYP1A1 mRNA), compared with the chimeric mouse's induced BaP hydroxylase activity (per unit of hCYP1A1 mRNA).

In contrast, B6 mice display about the same amount of TCDD-induced EROD activity (per unit of mCYP1A1 mRNA) as *uPA/SCID* mice (Table 2). The B6 mouse shows ~54 times more induced EROD activity (per unit of mCYP1A1 mRNA), compared with the *hCYP1A1_1A2_Cyp1a1/1a2(−/−)* mouse's induced EROD activity (per unit of hCYP1A1 mRNA). Chimeric mice exhibit ~1.7 times more induced EROD activity (per unit of hCYP1A1 mRNA) than *hCYP1A1_1A2_Cyp1a1/1a2(−/−)* mice (Table 2). The *uPA/SCID* mouse shows ~39 times more induced EROD activity (per unit of mCYP1A1 mRNA), compared with the chimeric mouse's induced EROD activity (per unit of hCYP1A1 mRNA).

Why does the humanized *hCYP1A1_1A2_Cyp1a1/1a2(−/−)* mouse carry so little enzyme activity toward BaP, compared with the chimeric mouse? This difference can be explained from the human hepatocyte-replacement rate (73%–83%) in chimeric mice. The liver of chimeric mice carries 73%–83% human hepatocytes, which exhibit extremely low BaP hydroxylase activity.

For acetanilide 4-hydroxylase and MROD as two activities associated predominantly with CYP1A2, the correlations between enzyme activities (Fig. 3B) and mRNA levels (Fig. 1B) are very much consistent with one another. B6 mice show virtually the same amount of TCDD-induced acetanilide 4-hydroxylase activity (per unit of mCYP1A2 mRNA) as *uPA/SCID* mice (Table 2). The B6 mouse shows about the same amount of induced acetanilide 4-hydroxylase activity (per unit of mCYP1A2 mRNA), compared with the *hCYP1A1_1A2_Cyp1a1/1a2(−/−)* mouse's induced acetanilide 4-hydroxylase activity (per unit of hCYP1A2 mRNA). Chimeric mice exhibit twice as much induced acetanilide 4-hydroxylase activity (per unit of hCYP1A2 mRNA) than *hCYP1A1_1A2_Cyp1a1/1a2(−/−)* mice (Table 2). The chimeric mouse shows ~2.3-fold more induced acetanilide 4-hydroxylase activity (per unit of mCYP1A2 mRNA), compared with the *uPA/SCID* mouse's induced acetanilide 4-hydroxylase activity (per unit of hCYP1A2 mRNA).

B6 mice exhibit one-half as much TCDD-induced MROD activity (per unit of mCYP1A2 mRNA) as *uPA/SCID* mice (Table 2). The *hCYP1A1_1A2_Cyp1a1/1a2(−/−)* mouse shows ~2-fold more induced MROD activity (per unit of mCYP1A2 mRNA), compared with the B6 mouse's induced MROD activity (per unit of hCYP1A2 mRNA). The *hCYP1A1_1A2_Cyp1a1/1a2(−/−)* mice exhibit ~2.4 times more in-

Table 2
Ratios of mouse liver TCDD-induced enzymic activities per unit of mRNA*.

	mCYP1A1		hCYP1A1	
B6 mouse	7600 ± 2700	h1A1_1A2	44 ± 13	BaP hydroxylase
uPA/SCID	11,400 ± 3000	Chimera	270 ± 62	
B6 mouse	230 ± 64	h1A1_1A2	4.3 ± 1.3	EROD activity
uPA/SCID	290 ± 95	Chimera	7.4 ± 3.1	
	mCYP1A2		**hCYP1A2**	
B6 mouse	490 ± 84	h1A1_1A2	600 ± 220	Acetanilide
uPA/SCID	510 ± 200	Chimera	1200 ± 390	4-hydroxylase
B6 mouse	5.4 ± 1.0	h1A1_1A2	14 ± 5.5	MROD activity
uPA/SCID	13 ± 5.2	Chimera	5.6 ± 0.3	

* For BaP hydroxylase, these ratios represent FU/min/mg protein divided by mRNA × 10^9 per μg total RNA. For the other three enzyme activities, these ratios represent pmol/min/mg protein divided by mRNA × 10^9 per μg total RNA. Values are expressed as means ± S.E.

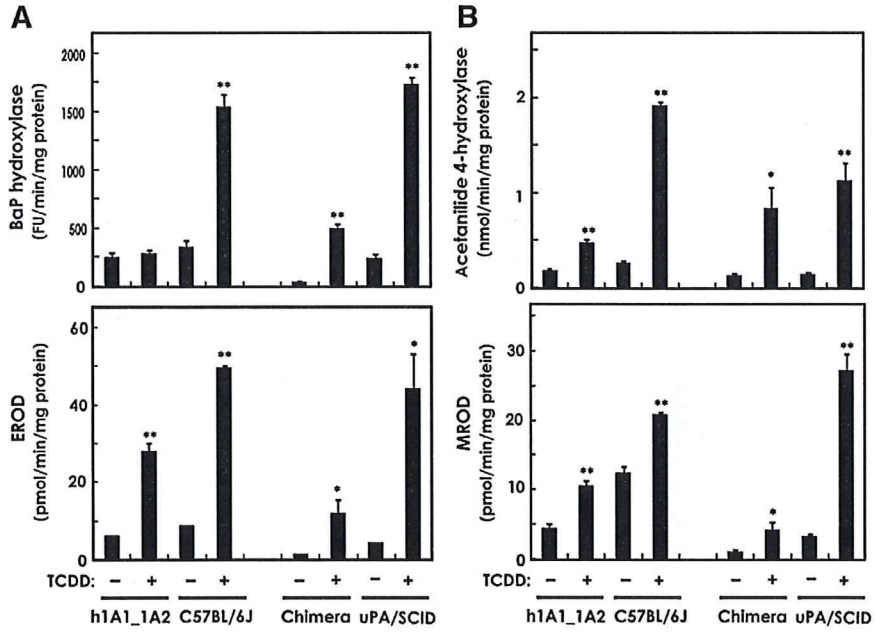

Fig. 3. (A) BaP hydroxylase and EROD activity (both representing largely CYP1A1), and (B) acetanilide 4-hydroxylase and MROD activity (both representing largely CYP1A2) in liver microsomes from the same mouse lines as in Fig. 1. FU, fluorescent units. *$P<0.05$ and **$P<0.01$, when comparing TCDD-pretreated with no pretreatment.

duced MROD activity (per unit of hCYP1A2 mRNA) than chimeric mice (Table 2). The *uPA/SCID* mouse shows twice as much induced MROD activity (per unit of mCYP1A2 mRNA), compared with the chimeric mouse's induced MROD activity (per unit of hCYP1A2 mRNA). Expression of CYP1A2 catalytic activity, relative to CYP1A2 mRNA levels, in the humanized *hCYP1A1_1A2_Cyp1a1/1a2(−/−)* and chimeric mouse lines is therefore very robust and within 2-fold similar to that expressed in mouse liver.

Comparison of human versus mouse CYP1A1 and CYP1A2 mRNA levels in hepatoma-derived cell culture lines

Animal rights' activists have urged scientists to study physiological functions in cell cultures rather than using live laboratory animals. Many studies have shown, however, that parameters found in cell culture do not accurately reflect what happens in the intact animal.

How does the expression of the *CYP1A1* and *CYP1A2* genes in intact liver compare with that in hepatoma-derived established cell lines? In HepG2 cells (Fig. 4A), human basal CYP1A1 mRNA was negligible, whereas human TCDD-induced CYP1A1 mRNA gave $\sim 5.4 \times 10^9$ copy numbers (per μg total RNA). In Hepa-1c1c7 cells (Fig. 4A), mouse basal versus TCDD-induced CYP1A1 mRNA showed $\sim 0.35 \times 10^8$ and $\sim 1.9 \times 10^8$ copy numbers, respectively. Mouse CYP1A1 mRNA was not detected in HepG2, and human CYP1A1 mRNA was not detected in Hepa-1c1c7 cells.

In HepG2 cells (Fig. 4B), human basal versus TCDD-induced CYP1A2 mRNA gave $\sim 0.27 \times 10^6$ and $\sim 4.8 \times 10^6$ copy numbers, respectively. In Hepa-1c1c7 cells (Fig. 4B), mouse basal versus TCDD-induced CYP1A2 mRNA showed $\sim 0.14 \times 10^6$ and $\sim 1.2 \times 10^6$ copies, respectively. Mouse CYP1A2 mRNA was not detected in HepG2, and human CYP1A2 mRNA was not detected in Hepa-1c1c7 cells.

Thus, in livers of the *hCYP1A1_1A2_Cyp1a1/1a2(−/−)* and chimeric mice, the copy number of human induced CYP1A1 mRNA is 7.5 and 2.6 times, respectively, greater than that of human induced CYP1A2 mRNA. On the other hand, in the HepG2 liver-derived established cell line, the copy number of human induced CYP1A1 mRNA is more than 1100 times greater than that of human induced CYP1A2 mRNA. In livers of the B6 and *uPA/SCID* mice, the copy number of mouse induced CYP1A2 mRNA is 40-fold and 20-fold, respectively, greater than that of mouse induced CYP1A1 mRNA; in contrast, in the Hepa-1c1c7 established cell line, the copy number of mouse induced CYP1A1 mRNA is almost 1600-fold greater than that of mouse maximally-inducible CYP1A2 mRNA. This decline in *CYP1A2* gene expression seen in established cell lines reflects the well-known fact that numerous "housekeeping" genes such as *CYP1A2* are extinguished, or are greatly decreased in expression—in tumor cells as well as "established", or transformed, cell lines in culture (Owens et al., 1975; Nebert, 2006). However, such suppression often does not occur for the *CYP1A1* gene in differentiated tumors, including the HepG2 and Hepa-1c1c7 hepatoma-derived cell lines (Owens et al., 1975; Nebert, 2006).

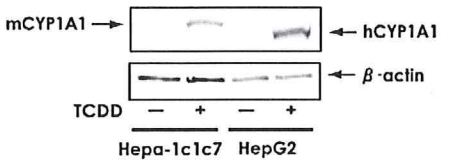

Fig. 5. Western immunoblot analysis of mouse versus human hepatic CYP1A1 and CYP1A2 proteins in the same cell culture lines as in Fig. 4. Everything is the same as that described for the Western blot in Fig. 2. The amount of cell culture protein (10 μg) loaded per lane was constant for all lanes.

Comparison of human versus mouse CYP1A1 and CYP1A2 protein levels in hepatoma-derived cell culture lines

We carried out Western immunoblots of Hepa-1c1c7 and HepG2 cells, control versus TCDD-pretreated (Fig. 5). The human CYP1A1 protein appears to migrate more rapidly than the mouse CYP1A1 protein. We believe the level of CYP1A2 protein was so low that it was not detected in either established hepatoma cell line.

Comparison of human versus mouse CYP1A1 and CYP1A2 TCDD-induced enzyme activities in hepatoma-derived cell culture lines

Different from what was found in mouse liver, the correlations between enzyme activities (Fig. 6A) and mRNA levels (Fig. 4A) are extremely variable for EROD activity but more consistent for BaP

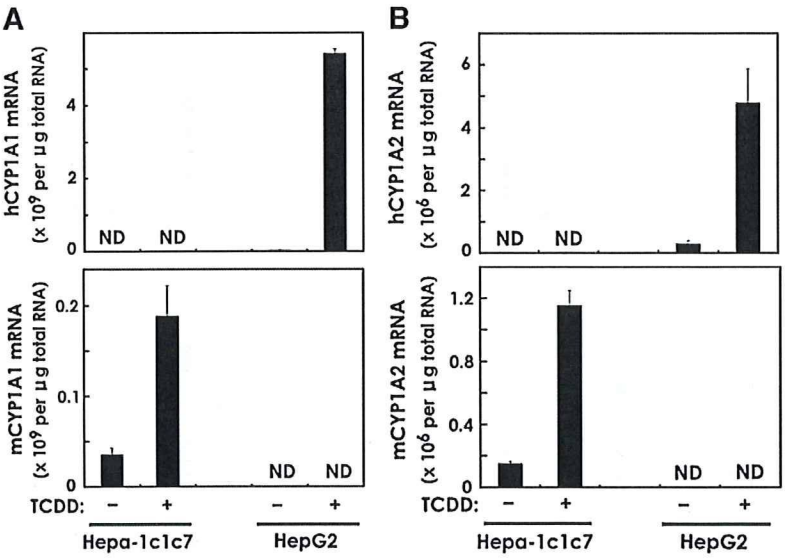

Fig. 4. Human (*upper panels*) versus mouse (*lower panels*) CYP1A1 (A) and CYP1A2 (B) mRNA copy numbers in mouse Hepa-1c1c7 cells and human HepG2 cells—with, versus without, TCDD exposure (10 nM for 24 h) in culture. Abbreviations are the same as those in Fig. 1.

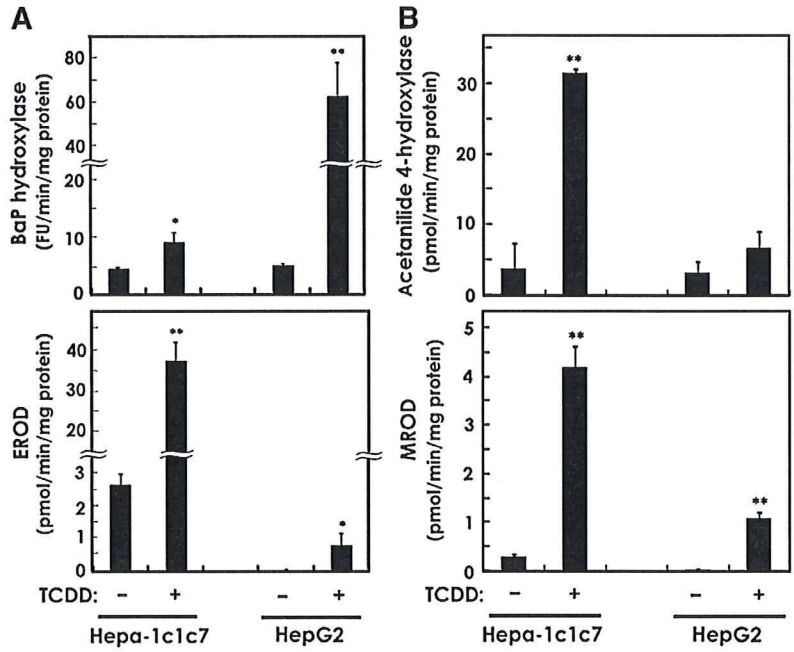

Fig. 6. (A) BaP hydroxylase and EROD activity (both representing largely CYP1A1), and (B) acetanilide 4-hydroxylase and MROD activity (both representing largely CYP1A2) in the same cell culture lines as in Fig. 4. *$P<0.05$ and **$P<0.01$, when comparing TCDD-pretreated with no pretreatment.

hydroxylase activity. Hepa-1c1c7 cells show ~4.8 times more TCDD-induced BaP hydroxylase activity (per unit of mCYP1A1 mRNA) than HepG2 cells exhibit for induced BaP hydroxylase activity (per unit of hCYP1A1 mRNA) (Table 3). Hepa-1c1c7 cells show ~1500 times more TCDD-induced EROD activity (per unit of mCYP1A1 mRNA) than HepG2 cells exhibit for induced EROD activity (per unit of hCYP1A1 mRNA). For whatever reason, HepG2 cells do not display very high induced BaP hydroxylase activity, and their induced EROD activity is extremely low.

For acetanilide 4-hydroxylase and MROD as two activities associated predominantly with CYP1A2, the correlations between enzyme activities (Fig. 6B) and mRNA levels (Fig. 6B) are better than those with CYP1A1. Hepa-1c1c7 cells show ~16-fold more TCDD-induced acetanilide 4-hydroxylase activity (per unit of mCYP1A2 mRNA) than HepG2 cells exhibit for induced acetanilide 4-hydroxylase activity (per unit of hCYP1A2 mRNA) (Table 3). Hepa-1c1c7 cells show ~15-fold more TCDD-induced MROD activity (per unit of mCYP1A2 mRNA) than HepG2 cells exhibit for induced MROD activity (per unit of hCYP1A2 mRNA). Therefore, HepG2 cells do not express either CYP1A1 or CYP1A2 activities nearly as robustly as do Hepa-1c1c7 cells.

Table 3
Ratios of hepatoma-derived cell line TCDD-induced enzymic activities per unit of mRNA*.

	mCYP1A1		hCYP1A1	
Hepa-1c1c7	55 ± 21	HepG2	11 ± 2.5	BaP hydroxylase
Hepa-1c1c7	210 ± 48	HepG2	0.14 ± 0.06	EROD activity
	mCYP1A2		**hCYP1A2**	
Hepa-1c1c7	27,000 ± 2400	HepG2	1800 ± 930	Acetanilide 4-hydroxylase
Hepa-1c1c7	3700 ± 480	HepG2	250 ± 85	MROD activity

* For BaP hydroxylase, these ratios represent FU/min/mg protein divided by mRNA × 10^9 per μg total RNA. For the other three enzyme activities, these ratios represent pmol/min/mg protein divided by mRNA × 10^9 per μg total RNA. Values are expressed as means ± S.E.

Conclusions

In this study we have measured the amount of variability between human and mouse CYP1A mRNA and protein levels and corresponding enzyme activities in the humanized *hCYP1A1_1A2_Cyp1a1/1a2(−/−)* and chimeric *uPA/SCID* lines, by comparing these parameters with those seen in wild-type mice from which these two lines were derived. We have also compared these mRNA and protein levels and corresponding enzyme activities in mouse hepatoma-derived Hepa-1c1c7 and human hepatoblastoma-derived HepG2 established cell culture lines. Clearly, the CYP1A1/CYP1A2 activity ratios in these hepatoma-derived established cell lines are not accurate indicators of those in liver from the intact mouse. Undoubtedly, this discrepancy is primarily caused by the dramatically lowered CYP1A2 mRNA levels—presumably due to "extinction" of the normal expression of the *CYP1A2* gene in these hepatoma-derived established cell lines. Not only very low CYP1A2 enzyme activity per unit of mRNA was seen in both Hepa-1c1c7 and HepG2 cells, but also low CYP1A1 enzyme activity per unit of hCYP1A1 mRNA was found in HepG2 cells.

Comparing liver of the two humanized mouse lines with liver of mice from which these two humanized lines were derived was most disturbing when one examined CYP1A1-specific (BaP and ethoxyresorufin) and CYP1A2-specific (acetanilide and methoxyresorufin) substrates metabolized—per unit of mCYP1A1, hCYP1A1, mCYP1A2 or hCYP1A2 mRNA. The hCYP1A1 in mouse liver was between 38 and more than 170 times less efficient than mCYP1A1 in the hydroxylation of BaP and about 54-fold less efficient in EROD activity. In contrast, hCYP1A2 in mouse liver appeared to function nearly equivalent to mCYP1A2 in wild-type mouse liver.

The levels of human CYP1A1 and CYP1A2 mRNA in both humanized mouse lines appear to be quite compatible with what might be expected among individual persons in any human population. It is very clear, however, that substrate specificity varies widely, independent of human versus mouse CYP1A1/1A2 mRNA or protein concentrations. Nevertheless, keeping this caveats in mind, both of these lines should still be useful for studies in human risk assessment, toxicology, pharmacology, and other medical subspecialties.

Note added in proof

A recent study (Wilson et al., 2008) is directly relevant to the problems addressed in our present manuscript. This study involves Tc1 hepatocytes, derived from an aneuploid mouse strain carrying human chromosome (Chr) 21 in addition to the entire mouse genome. The authors compared the regulation of human genes in Tc1 cells to that of the mouse orthologous genes in these same cells, using mouse wild-type versus human wild-type cells as controls. Regulation in the nuclei of Tc1 cells was compared at three levels: binding of transcription factors to DNA, modification of histones, and gene expression. The binding patterns of HNF1α, HNF4α and HNF6 on human Chr 21 in Tc1 cells matched closely those seen in human wild-type cells, rather than those seen in mouse wild-type cells. Similarly, histone modifications–as well as gene expression (the amount of mRNA transcribed)–showed human-specific, instead of mouse-specific, patterns on human Chr 21 in Tc1 cells. The authors concluded that it is the regulatory DNA sequence, rather than any other species-specific factor, which is the single most important determinant of gene expression (Wilson et al., 2008).

Acknowledgments

We thank our colleagues for many fruitful discussions and careful readings of this manuscript. Supported, in part, by the Ministry of Education, Science, Sports & Culture, Japan (Grant-in-Aid for Scientific Research on Priority Areas, 18077005 to S.U. and M.M.), and Nihon University Joint Research Grant for 2007 (S.U.), and NIH Grants R01 ES014403 (D.W.N.) and P30 ES06096 (D.W.N.).

References

Aoyama, T., Gonzalez, F.J., Gelboin, H.V., 1989. Human cDNA-expressed cytochrome P450 1A2: mutagen activation and substrate specificity. Mol. Carcinog. 2, 192–198.
Bedell, M.A., Jenkins, N.A., Copeland, N.G., 1996. Good genes in bad neighbourhoods. Nat. Genet. 12, 229–232.
Bennett, L.M., McAllister, K.A., Blackshear, P.E., Malphurs, J., Goulding, G., Collins, N.K., Ward, T., Bunch, D.O., Eddy, E.M., Davis, B.J., Wiseman, R.W., 2000. *Brca2*-null embryonic survival is prolonged on the BALB/c genetic background. Mol. Carcinog. 28, 174–183.
Bernhard, H.P., Darlington, G.J., Ruddle, F.H., 1973. Expression of liver phenotypes in cultured mouse hepatoma cells: synthesis and secretion of serum albumin. Dev. Biol. 35, 83–96.
Berthou, F., Guillois, B., Riche, C., Dreano, Y., Jacqz-Aigrain, E., Beaune, P.H., 1992. Interspecies variations in caffeine metabolism related to cytochrome P450 1A enzymes. Xenobiotica 22, 671–680.
Bonyadi, M., Rusholme, S.A., Cousins, F.M., Su, H.C., Biron, C.A., Farrall, M., Akhurst, R.J., 1997. Mapping of a major genetic modifier of embryonic lethality in *Tgfb1(−/−)* knockout mice. Nat. Genet. 15, 207–211.
Burke, M.D., Mayer, R.T., Kouri, R.E., 1977. 3-Methylcholanthrene-induced monooxygenase (*O*-deethylation) activity of human lymphocytes. Cancer Res. 37, 460–463.
Cheung, C., Ma, X., Krausz, K.W., Kimura, S., Feigenbaum, L., Dalton, T.P., Nebert, D.W., Idle, J.R., Gonzalez, F.J., 2005. Differential metabolism of 2-amino-1-methyl-6-phenylimidazo[4,5-*b*]pyridine (PhIP) in mice humanized for CYP1A1 and CYP1A2. Chem. Res. Toxicol. 18, 1471–1478.
Cranston, A., Fishel, R., 1999. Female embryonic lethality in *Msh2–Trp53* nullizygous mice is strain-dependent. Mamm. Genome 10, 1020–1022.
Dalton, T.P., Dieter, M.Z., Matlib, R.S., Childs, N.L., Shertzer, H.G., Genter, M.B., Nebert, D.W., 2000. Targeted knockout of *Cyp1a1* gene does not alter hepatic constitutive expression of other genes in the mouse [*Ah*] battery. Biochem. Biophys. Res. Commun. 267, 184–189.
Dearfield, K.L., Jacobson-Kram, D., Brown, N.A., Williams, J.R., 1983. Evaluation of a human hepatoma cell line as a target cell in genetic toxicology. Mutat. Res. 108, 437–449.
Derkenne, S., Curran, C.P., Shertzer, H.G., Dalton, T.P., Dragin, N., Nebert, D.W., 2005. Theophylline pharmacokinetics: comparison of *Cyp1a1(−/−)* and *Cyp1a2(−/−)* knockout mice, humanized *hCYP1A1_1A2* knock-in mice lacking either the mouse *Cyp1a1* or *Cyp1a2* gene, and *Cyp1(+/+)* wild-type mice. Pharmacogenet. Genomics 15, 503–511.
Dragin, N., Uno, S., Wang, B., Dalton, T.P., Nebert, D.W., 2007. Generation of 'humanized' *hCYP1A1_1A2_Cyp1a1/1a2(−/−)* mouse line. Biochem. Biophys. Res. Commun. 359, 635–642.
Eaton, D.L., Gallagher, E.P., Bammler, T.K., Kunze, K.L., 1995. Role of cytochrome P450 1A2 in chemical carcinogenesis: implications for human variability in expression and enzyme activity. Pharmacogenetics 5, 259–274.
Giannini, C., Morosan, S., Tralhao, J.G., Guidotti, J.E., Battaglia, S., Mollier, K., Hannoun, L., Kremsdorf, D., Gilgenkrantz, H., Charneau, P., 2003. A highly efficient, stable, and rapid approach for ex vivo human liver gene therapy via a FLAP lentiviral vector. Hepatology 38, 114–122.
Hamm, J.T., Ross, D.G., Richardson, V.M., Diliberto, J.J., Birnbaum, L.S., 1998. Methoxyresorufin: an inappropriate substrate for CYP1A2 in the mouse. Biochem. Pharmacol. 56, 1657–1660.
Inaba, Y., Yamamoto, K., Yoshimoto, N., Matsunawa, M., Uno, S., Yamada, S., Makishima, M., 2007. Vitamin D3 derivatives with adamantane or lactone ring side chains are cell type-selective vitamin D receptor modulators. Mol. Pharmacol. 71, 1298–1311.
Jiang, Z., Dalton, T.P., Jin, L., Wang, B., Tsuneoka, Y., Shertzer, H.G., Deka, R., Nebert, D.W., 2005. Toward the evaluation of function in genetic variability: characterizing human SNP frequencies and establishing BAC-transgenic mice carrying the human *CYP1A1_CYP1A2* locus. Hum. Mutat. 25, 196–206.
Katoh, M., Tateno, C., Yoshizato, K., Yokoi, T., 2008. Chimeric mice with humanized liver. Toxicology 246, 9–17.
Lindberg, R.L., Negishi, M., 1989. Alteration of mouse cytochrome P450coh substrate specificity by mutation of a single amino-acid residue. Nature 339, 632–634.
Milot, E., Fraser, P., Grosveld, F., 1996. Position effects and genetic disease. Trends Genet. 12, 123–126.
Muller, K., Heller, H., Doerfler, W., 2001. Foreign DNA integration. Genome-wide perturbations of methylation and transcription in the recipient genomes. J. Biol. Chem. 276, 14271–14278.
Nebert, D.W., 1989. The *Ah* locus: genetic differences in toxicity, cancer, mutation, and birth defects. Crit. Rev. Toxicol. 20, 153–174.
Nebert, D.W., 2006. Comparison of gene expression in cell culture to that in the intact animal: relevance to drugs and environmental toxicants. Am. J. Physiol., Cell Physiol. 290, C37–C41.
Nebert, D.W., Dalton, T.P., 2006. The role of cytochrome P450 enzymes in endogenous signalling pathways and environmental carcinogenesis. Nat. Rev., Cancer 6, 947–960.
Nebert, D.W., Gelboin, H.V., 1968. Substrate-inducible microsomal aryl hydroxylase in mammalian cell culture. I. Assay and properties of induced enzyme. J. Biol. Chem. 243, 6242–6249.
Nebert, D.W., Dalton, T.P., Okey, A.B., Gonzalez, F.J., 2004. Role of aryl hydrocarbon receptor-mediated induction of the CYP1 enzymes in environmental toxicity and cancer. J. Biol. Chem. 279, 23847–23850.
Nelson, D.R., Koymans, L., Kamataki, T., Stegeman, J.J., Feyereisen, R., Waxman, D.J., Waterman, M.R., Gotoh, O., Coon, M.J., Estabrook, R.W., Gunsalus, I.C., Nebert, D.W., 1996. P450 superfamily: update on new sequences, gene mapping, accession numbers and nomenclature. Pharmacogenetics 6, 1–42.
Nelson, D.R., Zeldin, D.C., Hoffman, S.M., Maltais, L.J., Wain, H.M., Nebert, D.W., 2004. Comparison of cytochrome P450 (*CYP*) genes from the mouse and human genomes, including nomenclature recommendations for genes, pseudogenes, and alternative-splice variants. Pharmacogenetics 14, 1–18.
Nichols, R.C., Cooper, S., Trask, H.W., Gorman, N., Dalton, T.P., Nebert, D.W., Sinclair, J.F., Sinclair, P.R., 2003. Uroporphyrin accumulation in hepatoma cells expressing human or mouse CYP1A2: relation to the role of CYP1A2 in human porphyria cutanea tarda. Biochem. Pharmacol. 65, 545–550.
Olson, E.N., Arnold, H.H., Rigby, P.W., Wold, B.J., 1996. Know your neighbors: three phenotypes in null mutants of the myogenic bHLH gene *Mrf4*. Cell 85, 1–4.
Owens, I.S., Niwa, A., Nebert, D.W., 1975. In: Gerschenson, L.E., Thompson, E.B. (Eds.), Expression of Aryl Hydrocarbon Hydroxylase Induction in Liver- and Hepatoma-Derived Cell Cultures. Academic Press, New York, NY, pp. 378–401.
Shertzer, H.G., Nebert, D.W., Senft, A.P., Dingledein, M., Genter, M.B., Dalton, T.P., 2001. Spectrophotometric assay for acetanilide 4-hydroxylase, an estimate of CYP1A2 enzyme activity. Toxicol. Meth. 11, 81–88.
Shi, Z., Chen, Y., Dong, H., Amos-Kroohs, R.M., Nebert, D.W., 2008. Generation of 'humanized' *hCYP1A1_1A2_Cyp1a1/1a2(−/−)_Ahr^d* mouse line harboring the poor-affinity aryl hydrocarbon receptor. Biochem. Biophys. Res. Commun. 376, 775–780.
Tateno, C., Yoshizane, Y., Saito, N., Kataoka, M., Utoh, R., Yamasaki, C., Tachibana, A., Soeno, Y., Asahina, K., Hino, H., Asahara, T., Yokoi, T., Furukawa, T., Yoshizato, K., 2004. Near completely humanized liver in mice shows human-type metabolic responses to drugs. Am. J. Pathol. 165, 901–912.
Tavangar, K., Hoffman, A.R., Kraemer, F.B., 1990. A micromethod for the isolation of total RNA from adipose tissue. Anal. Biochem. 186, 60–63.
Turesky, R.J., 2005. Interspecies metabolism of heterocyclic aromatic amines and the uncertainties in extrapolation of animal toxicity data for human risk assessment. Mol. Nutr. Food Res. 49, 101–117.
Uno, S., Dalton, T.P., Dragin, N., Curran, C.P., Derkenne, S., Miller, M.L., Shertzer, H.G., Gonzalez, F.J., Nebert, D.W., 2006. Oral benzo[*a*]pyrene in *Cyp1* knockout mouse lines: CYP1A1 important in detoxication, CYP1B1 metabolism required for immune damage independent of total-body burden and clearance rate. Mol. Pharmacol. 69, 1103–1114.
Uno, S., Dragin, N., Miller, M.L., Dalton, T.P., Gonzalez, F.J., Nebert, D.W., 2008. Basal and inducible CYP1 mRNA quantitation and protein localization throughout the mouse gastrointestinal tract. Free Radic. Biol. Med. 44, 570–583.
Wilson, M.D., Barbosa-Morais, N.L., Schmidt, D., Conboy, C.M., Vanes, L., Tybulewicz, V.L., Fisher, E.M., Tavaré, S., Odom, D.T., 2008. Species-specific transcription in mice carrying human chromosome 21. Science 322, 434–438.
Winer, J., Jung, C.K., Shackel, I., Williams, P.M., 1999. Development and validation of real-time quantitative reverse transcriptase-polymerase chain reaction for monitoring gene expression in cardiac myocytes in vitro. Anal. Biochem. 270, 41–49.

Inhibition of Transforming Growth Factor β Signaling by Halofuginone as a Modality for Pancreas Fibrosis Prevention

Orit Zion, MSc, Olga Genin, MSc,* Norifumi Kawada, MD,† Katsutoshi Yoshizato, MD,‡ Suzy Roffe, MsC,§ Arnon Nagler, MD,|| Juan L. Iovanna, MD, PhD,¶ Orna Halevy, PhD,§ and Mark Pines, PhD**

Objectives: Chronic pancreatitis is characterized by inflammation and fibrosis. We evaluated the efficacy of halofuginone, an inhibitor of collagen synthesis and myofibroblast activation, in preventing cerulein-induced pancreas fibrosis.

Methods: Collagen synthesis was evaluated by in situ hybridization and staining. Levels of prolyl 4-hydroxylase β (P4Hβ), cytoglobin/stellate cell activation–associated protein (Cygb/STAP), transgelin, tissue inhibitors of metalloproteinases, serum response factor, transforming growth factor β (TGFβ), Smad3, and pancreatitis-associated protein 1 (PAP-1) were determined by immunohistochemistry. Metalloproteinase activity was evaluated by zymography.

Results: Halofuginone prevented cerulein-dependent increase in collagen synthesis, collagen cross-linking enzyme P4Hβ, Cygb/STAP, and tissue inhibitors of metalloproteinase 2. Halofuginone did not affect TGFβ levels in cerulein-treated mice but inhibited serum response factor synthesis and Smad3 phosphorylation. In culture, halofuginone inhibited pancreatic stellate cell (PSC) proliferation and TGFβ-dependent increase in Cygb/STAP and transgelin synthesis and metalloproteinase 2 activity. Halofuginone increased c-Jun N-terminal kinase phosphorylation in PSCs derived from cerulein-treated mice. Halofuginone prevented the increase in acinar cell proliferation and further increased the cerulein-dependent PAP-1 synthesis.

Conclusions: Halofuginone inhibits Smad3 phosphorylation and increases c-Jun N-terminal kinase phosphorylation, leading to the inhibition of PSC activation and consequent prevention of fibrosis. Halofuginone increased the synthesis of PAP-1, which further reduces pancreas fibrosis. Thus, halofuginone might serve as a novel therapy for pancreas fibrosis.

Key Words: myofibroblasts, pancreatic stellate cells, Smad, collagen, transgelin, cytoglobin

(*Pancreas* 2009;38: 427–435)

Chronic pancreatitis is a progressive disease, characterized by inflammation, fibrosis, and atrophy of the gland tissue, which results in impaired exocrine and endocrine functions of the pancreas.[1] The cellular mechanisms governing pancreas fibrosis are shared among the various insults and, in many aspects, mirror the scarring and wound-healing processes of other tissues. Pancreas fibrosis, regardless of the cause, is characterized by an increase in extracellular matrix (ECM) constituents, although their relative distribution within the pancreas varies with the site and nature of the insult.[2] In the injured pancreas, the pancreatic stellate cells (PSCs) constitute the major source of ECM proteins.[3] These cells are usually quiescent, with a low proliferation rate; however, upon activation, they differentiate into myofibroblastlike cells with high proliferative capacity. The activated PSCs migrate to sites of tissue damage, where they synthesize ECM components to promote tissue repair.[4] The intracellular signaling mechanisms regulating PSC activation include the mitogen-activated protein kinase (MAPK) pathway, which plays a major role in ethanol- and acetaldehyde-dependent activation of PSC, phosphatidylinositol-3-kinase, and protein kinase C.[5]

The transition to the myofibroblastlike phenotype is associated with increased expression of specific smooth muscle genes such as α smooth muscle actin and transgelin (SM22α) and of specific markers such as cytoglobin/stellate cell activation–associated protein (Cygb/STAP) in fibrotic lesions of the pancreas.[6] Pancreatic stellate cells can be activated directly by alcohol consumption[7] or by cytokines derived from the immigrating inflammatory cells.[8,9] Platelet-derived growth factor is the major promoter of PSC migration, whereas transforming growth factor β (TGFβ) affects ECM production via a Smad-associated pathway. Upon phosphorylation by the TGFβ receptor, Smad3 enters the nucleus to modulate the transcription of target genes.[10] Smad3 links TGFβ signaling directly to the serum response factor (SRF)–associated regulatory network that controls the expression of smooth muscle–specific genes.[11,12] The predominant ECM protein synthesized by the PSCs is collagen type I, although increases in the gene expression of other types of collagens and other matrix proteins have also been reported.[13] Pancreas fibrosis may also result from a relative imbalance between the production and degradation of matrix proteins.[14] The PSCs constitute the source of various matrix metalloproteinases (MMPs) and tissue inhibitors of MMPs (TIMPs), which are necessary for ECM remodeling under the control of TGFβ.[15,16]

In addition to the morbidity and mortality caused by chronic pancreatitis, patients with this disease also have a substantially increased risk of developing pancreatic cancer. The PSCs play a major role in the growth and development of pancreas adenocarcinoma, which has a remarkable fibrotic component regulated by the TGFβ pathway.[4,17,18] The desmoplasia is created by activated PSCs, which are stimulated by the cancer cells, thereby influencing tumor aggressiveness.[19] Given that activated PSCs not only are the principal effector cells in pancreas fibrosis but also play a major role in pancreas carcinoma, it seems that targeting the fibroblast-to-PSC transition might be a promising therapeutic approach, for which there is a great unmet need.

From the *Institute of Animal Sciences, The Volcani Center, Bet Dagan, Israel; †Department of Hepatology, Graduate School of Medicine, Osaka City University, Japan; ‡Developmental Biology Laboratory, CLUSTER Project, and 21st Century COE Program, Department of Biological Science, Graduate School of Science, Hiroshima University, Japan; §Department of Animal Sciences, The Hebrew University of Jerusalem, Rehovot, Israel; ||Department of Hematology and Bone Marrow Transplantation, Chaim Sheba Medical Center, Tel Hashomer, Israel; and ¶INSERM U624, Stress Cellulaire, Campus de Luminy, Marseille, France.

Received for publication July 23, 2008; accepted November 24, 2008.

Reprints: Mark Pines, PhD, Institute of Animal Science, ARO, The Volcani Center, Bet Dagan 50250, Israel (e-mail: pines@agri.huji.ac.il).

Halofuginone, an analog of the plant alkaloid febrifugine, has been found to inhibit the activation of hepatic stellate cells (HSCs)[20,21] and the stromal fibroblast-to-myofibroblast transition in the tumor microenvironment.[22] Halofuginone overcame TGFβ-induced collagen synthesis by inhibiting Smad3 phosphorylation downstream of the TGFβ signaling pathway.[23] In animal models in which excess collagen is the hallmark of the disease, halofuginone prevented the increase in collagen synthesis. These models included mice afflicted with chronic graft-versus-host disease and tight-skin mice, rats with pulmonary fibrosis, and rats that developed adhesions at various sites.[23–25] When given to rats that exhibited established fibrosis, halofuginone caused almost a complete resolution of the fibrotic condition.[20] In addition, halofuginone markedly improved the capacity of a cirrhotic liver to regenerate after partial hepatectomy[26] by affecting the expression of early genes of liver regeneration under the control of TGFβ.[27,28] Topical treatment with halofuginone of a patient with chronic graft-versus-host disease and of patients with scleroderma elicited a transient attenuation of collagen α_1(I) gene expression and improvements in skin scores, thus demonstrating human clinical efficacy.[25,29]

In the present study, we evaluated the efficacy of halofuginone in inhibiting pancreas fibrosis in mice, with particular emphasis on TGFβ-dependent PSC activation and ECM production.

MATERIALS AND METHODS

Materials

Halofuginone bromhydrate was obtained from Collgard Biopharmaceuticals Ltd (Tel Aviv, Israel). Cerulein and β-casein were from Sigma (St Louis, Mo). Antibodies to Cygb/STAP were prepared according to Nakatani et al.[6] Smad3 and phosphorylated Smad3 (P-Smad3) antibodies were from Abcam (Cambridge, United Kingdom). Serum response factor antibodies were from Santa Cruz Biotechnology Inc (Santa Cruz, Calif). The proliferating cell nuclear antigen (PCNA) staining kit was from Zymed Laboratories (San Francisco, Calif). Metalloproteinase 2 and P4Hβ monoclonal antibodies were from Acris (Hiddenhausen, Germany), and TIMP1 and TIMP2 monoclonal antibodies were from Lab Vision (Fremont, Calif). Polyclonal antibodies to phospho-Akt (S^{473}P-AKT), phospho-ERK/MAPK (P-p44), total Akt and total ERK/MAPK (p44), and monoclonal antibody to total c-Jun N-terminal kinase (JNK) 1 were from Cell Signaling Technologies (Danvers, Mass). Active-JNK (P-JNK1) and active p38 (P-p38) antibodies were from Promega (Madison, Wis). Rabbit polyclonal antibodies against human pancreatitis-associated protein 1 (PAP-1) were prepared as described previously.[30]

Animal Model of Pancreas Fibrosis

Male ICR mice (Harlan Laboratories, Jerusalem, Israel) were kept under standard conditions with free access to water and chow. Fibrosis was induced in mice (n = 10) by repeated (every 6 h) intraperitoneal injections of cerulein (50 μg/kg) twice weekly for 4 or 8 weeks according to Neuschwander-Tetri et al.[31] Halofuginone was administered intraperitoneally to mice (n = 10) at 4 μg per animal, 3 times per week as described by Bruck et al,[20] starting at the same time as the cerulein. Untreated mice (n = 10) and mice treated only with halofuginone (n = 10) were used as controls. All animal experiments were carried out according to the guidelines of the Volcani Center Institutional Committee for Care and Use of Laboratory Animals (Bet Dagan, Israel).

Preparation of Sections, In Situ Hybridization, and Immunohistochemistry

Pancreas samples were fixed overnight in 4% paraformaldehyde in phosphate-buffered saline at 4°C. Serial 5-μm sections were prepared after the samples had been embedded in Paraplast (McCormick Scientific, St Louis, Mo). Collagenous and noncollagenous proteins were differentially stained with 0.1% Sirius red and 0.1% Fast green as a counterstain, in saturated picric acid. By this procedure, collagen is stained red. Collagen levels were quantified by image analysis (ImagePro; Media Cybernetics, Silver Spring, Md). At least 20 photographs were taken for each analysis per each treatment at each time point. The results were calculated as the red area divided by the total red and green area and presented as arbitrary units of the mean (SE). Special care was taken to exclude the blank areas, which probably represented artifacts. In situ hybridization with a digoxigenin-labeled collagen α_1(I) probe was performed as described by Bruck et al.[20] No signal was observed with the sense probe. For immunohistochemistry, the following antibodies were used: SRF (diluted 1:500), TGFβ1 (1:400), Cygb/STAP (1:700), Smad3 (1:200), P-Smad2/3 (1:700), P4Hβ (1:25), TIMP1 (1:50), TIMP2 (1:250), and PAP-1 (1:10). In all cases, at least 5 slides from all the animals within the group were evaluated blindly to the animal grouping.

Cell Culture

Pancreatic stellate cells were prepared from either control mice or mice treated with a single injection of cerulein (50 μg/kg). After 24 hours, the pancreas was excised, freed from fat and lymph nodes, and digested with collagenase IV (0.02%), and the resulting cell suspension was centrifuged at 1200*g* for 5 minutes. The cells were washed and resuspended in Dulbecco's modified essential medium (DMEM) containing 10% fetal bovine serum and antibiotics (100-U/mL penicillin, 100-mg/mL streptomycin) and plated on 6-well plates with the same medium.[32] No significant differences were observed in the cell yield between the control and cerulein-treated mice, and almost all the cells were stained positive for Cygb/STAP or SM22α. All of the cells were incubated at 37°C in a humidified atmosphere containing 5% carbon dioxide. The cells were incubated with serum-free DMEM for 6 hours and were then treated with fresh medium containing halofuginone (20 or 50 nmol/L), TGFβ (3 ng/mL), or both for an additional 24 hours. Cellular viability was determined by trypan blue exclusion. At the end of the incubation period, the cells were either counted directly with a cell counter (Coulter Electronics, Bath, United Kingdom) or resuspended in 500 μL of lysis buffer consisting of 1-mmol/L EDTA, 50-mmol/L Tris (pH, 7.5), 150-mmol/L NaCl, 10% glycerol, 1% Nonidet P40, and a 1:100 dilution of protease and phosphatase inhibitor cocktail (Sigma).

Western Blot

Protein lysate (30 μg) from either tissue or cells was electrophoresed on a 10% sodium dodecyl sulfate–polyacrylamide gel and transferred onto a nitrocellulose membrane. Nonspecific binding sites were blocked with 5% low-fat milk, and the membranes were incubated overnight with the appropriate antibodies for SM22α (1:5000), Cygb/STAP (1:1000), MMP-2 (1:200), phospho-Akt (1:1000), phosphor–ERK/MAPK (1:2000), total Akt and total ERK/MAPK (1:1500), active

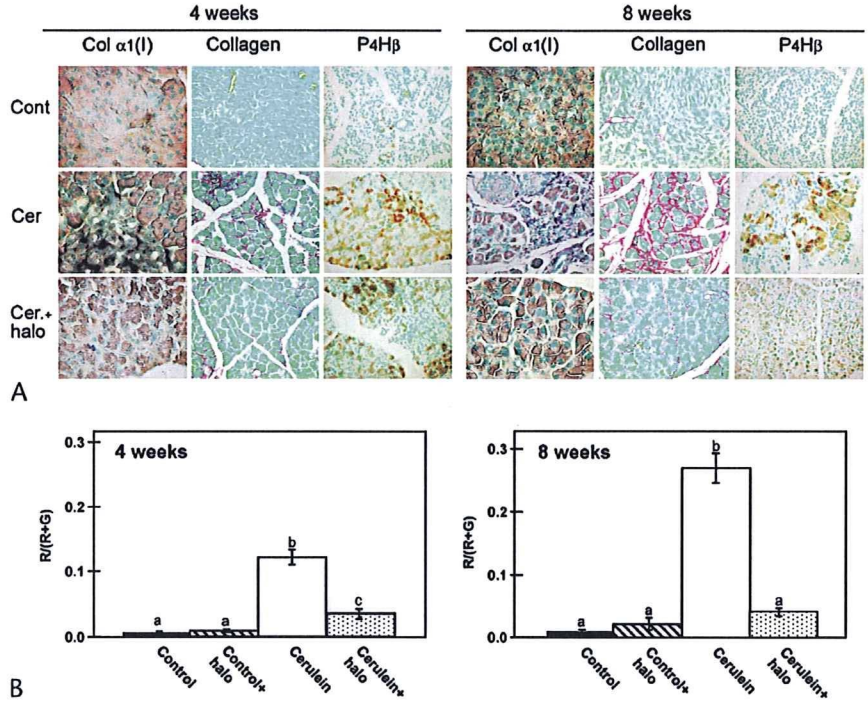

FIGURE 1. Effect of halofuginone on cerulein-dependent synthesis of collagen and P4Hβ, a collagen cross-linking enzyme. Mice were treated with cerulein for 4 or 8 weeks with or without halofuginone, after which pancreas biopsies were taken for histology. A, Collagen α_1(I) gene expression was determined by in situ hybridization, collagen level was evaluated by Sirius red staining, and P4Hβ was determined by immunohistochemistry. B, Image analysis of pancreas collagen levels. In each column, means without a common letter differ significantly ($P < 0.05$) according to Duncan multiple range test.

JNK (1:5000), active p38 (1:2000), and monoclonal antibody to total JNK (1:1000).

Zymography

Conditioned medium samples were analyzed for MMP activity, which was determined in a 10% sodium dodecyl sulfate–polyacrylamide gel impregnated with gelatin (0.01%) or β-casein (1.0 mg/mL). Proteins were separated on the gel under nonreducing conditions, followed by 1 hour of incubation in 2.5% Triton X-100 and 16 hours of incubation in 50-mmol/L Tris (pH, 7.6), 0.2-mol/L NaCl, and 5-mmol/L $CaCl_2$ at 37°C. After the incubation period, the gels were stained with 0.5% Coomassie G 250 in methanol/acetic acid/water (30:10:60, vol/vol/vol).

Statistical Analysis

The results are presented as the mean (SD). The significance of differences among different groups was determined by analysis of variance. In each column, means without a common letter differ significantly ($P < 0.05$) according to Duncan multiple range test.

RESULTS

Halofuginone Inhibits Pancreas Fibrosis

Pancreas fibrosis is the result of a dynamic cascade of mechanisms beginning with acinar cell injury and followed by inflammation and PSC activation. After 4 weeks of cerulein treatment, we observed a major increase in the number of PSCs expressing the collagen α_1(I) gene, the synthesis of large quantities of collagen surrounding the acinar cells, and positive staining for P4Hβ, one of the major enzymes responsible for collagen cross-linking and maturation (Fig. 1A). Collagen accumulated in the pancreas with time, and after an additional 4 weeks of cerulein treatment, a further increase in collagen content and P4Hβ level was observed. Halofuginone prevented the increase in fibrosis in a time-dependent fashion, as demonstrated by reductions in the expression of the collagen α_1(I) gene, in collagen content, and in the level of P4Hβ. After 4 weeks of halofuginone treatment, the collagen level was significantly lower than that of the cerulein-treated mice but was still higher than that of the control mice. After 8 weeks of halofuginone treatment, the collagen level was significantly lower than that of the cerulein-treated mice and did not differ from that of the control untreated mice (Fig. 1B). Halofuginone alone had no effect on the collagen content or other histologic parameters in the control untreated mice (data not shown).

Halofuginone Inhibits PSC Activation

In addition to enhancing collagen synthesis, activated PSCs are also characterized by increased proliferation and expression of SM22α and Cygb/STAP genes under the control of TGFβ. After 4 weeks of cerulein treatment, a major increase in the number of PSCs exhibiting Cygb/STAP was observed, which persisted for at least 8 weeks. Halofuginone reduced the number of Cygb/STAP-positive cells in the pancreas (Fig. 2A) and inhibited the TGFβ-induced Cygb/STAP levels in primary PSCs in cultures derived from the pancreas of control and cerulein-treated mice (Fig. 2B). Transgelin is induced during transdifferentiation of fibroblasts to myofibroblasts at the time of stromal tissue remodeling under the

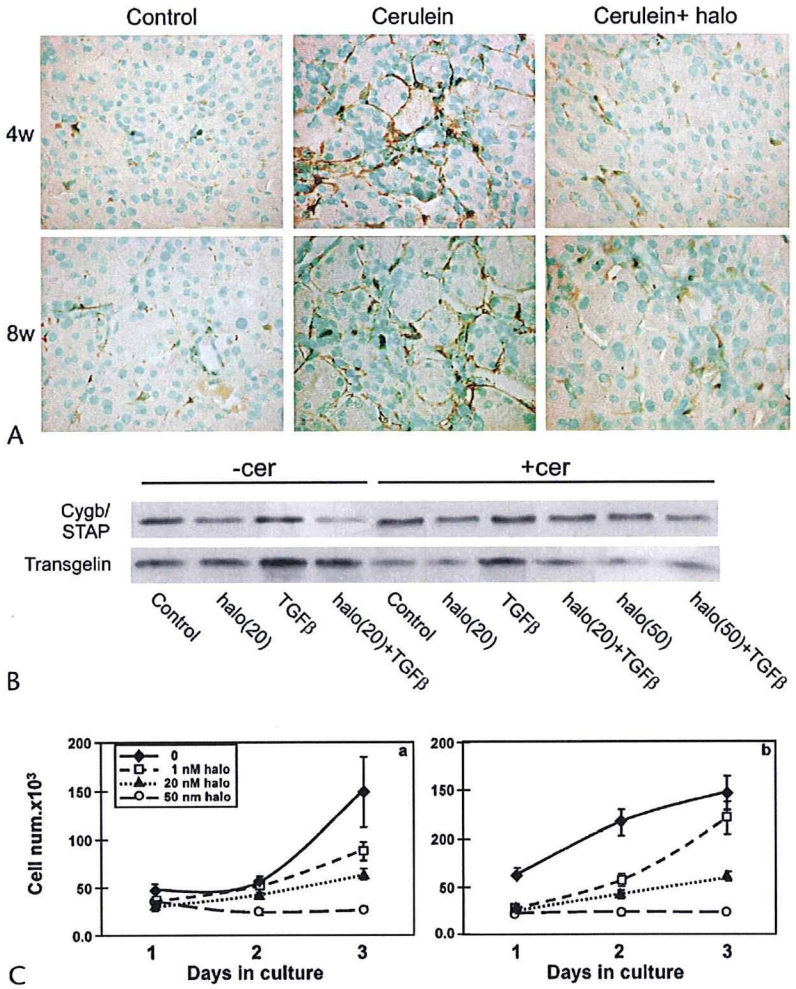

FIGURE 2. Effect of halofuginone on the synthesis of Cygb/STAP and SM22α and on PSC proliferation. A, Immunohistochemistry of Cygb/STAP in pancreas biopsies of mice treated for 4 or 8 weeks with cerulein, with or without halofuginone. B, Western blotting of Cygb/STAP and SM22α of PSCs derived from either control or cerulein-treated mice. The cells were incubated for 18 hours with TGFβ (3 ng/mL), halofuginone, or their combination. C, Primary PSCs were incubated with various concentrations of halofuginone, and cell proliferation was estimated directly by cell counting.

control of TGFβ. The PSCs in culture from control and cerulein-treated mice synthesized SM22α, which was upregulated by TGFβ. Halofuginone prevented the TGFβ-dependent SM22α synthesis in cultured primary PSCs derived from either control or cerulein-treated mice (Fig. 2B). The inhibitory effect of halofuginone on Cygb/STAP and SM22α synthesis was accompanied by a dose-dependent inhibition of proliferation of PSCs derived from either the normal pancreas or cerulein-treated mice (Fig. 2C). All of these findings were consistent with halofuginone inhibition of PSC activation.

Halofuginone and Matrix Degradation

The levels of TIMP1 and TIMP2 were increased in the pancreas after cerulein treatment, but only the TIMP2 level was inhibited by halofuginone (Fig. 3A). Metalloproteinase 2 is one of the major MMPs involved in pancreas fibrosis under the control of TGFβ.[14–16] Halofuginone had only a minimal, if any, effect on MMP-2 levels in the control mice. Cerulein treatment caused an increase in MMP-2 levels, which were further increased after halofuginone treatment (Fig. 3B). In culture, a major increase in basal MMP-2 activity was observed in conditioned medium of PSCs derived from cerulein-treated mice compared with controls (Fig. 3C). Halofuginone had no effect on the basal level of MMP-2 activity but inhibited the TGFβ-dependent increase in its activity by PSCs derived from control and cerulein-treated mice (Fig. 3D). In contrast, halofuginone increased MMP-3 activity, but only in PSCs derived from cerulein-treated mice (Fig. 3E).

Halofuginone Inhibits TGFβ Signaling

Almost no TGFβ was observed in the control untreated pancreas, whereas in the cerulein-treated mice, a major increase in its level was observed, mostly in the acinar cells but also in some of the PSCs (Fig. 4). Halofuginone treatment did not cause any change in the level of TGFβ, in agreement with previous studies suggesting that halofuginone affects TGFβ signaling downstream in its pathway.[23] Halofuginone treatment eliminated the synthesis of SRF, which was observed exclusively in the PSCs of the cerulein-treated pancreas. In the untreated pancreas, Smad3 was observed only in endothelial cells

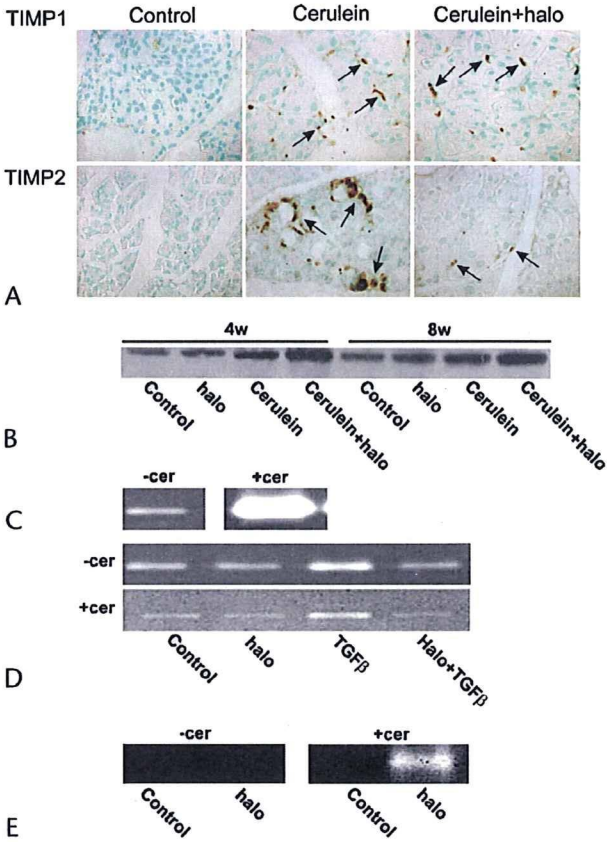

FIGURE 3. Halofuginone and the ECM degradation pathway. A, Immunohistochemistry of TIMP1 and TIMP2 in the pancreas after 8 weeks of cerulein treatment, with or without halofuginone. B, Western blotting with MMP-2 antibodies of pancreas extracts. C, Gelatin zymography for evaluation of MMP-2 activity in conditioned medium of PSCs derived from the cerulein-treated or untreated pancreas. Note the high levels of MMP-2 activity in conditioned medium of PSCs derived from the cerulein-treated pancreas. D, Effect of halofuginone on MMP-2 activity. E, Metalloproteinase 3 in conditioned medium collected from PSCs derived from the normal and the cerulein-treated pancreas.

surrounding the blood vessels, and no P-Smad3 was observed in any cell type. After cerulein treatment, increases in Smad3 and P-Smad3 were observed. Smad3 was observed mostly in the PSCs, whereas P-Smad3 was observed in the acinar cells and the PSCs. Halofuginone had no effect on the level of Smad3 protein expression, whereas complete elimination of P-Smad3 was observed after halofuginone treatment (Fig. 4).

Intracellular PSC Signaling Is Affected by Halofuginone

We evaluated the effect of halofuginone on the phosphorylation of key proteins in the MAPK pathways—JNK, MAPK/ERK, and p38 MAPK—and on Akt in PSCs derived from the control and the cerulein-treated pancreas (Fig. 5). Levels of phosphorylated JNK and, to a much lesser extent, phosphorylated MAPK/ERK were higher in the PSCs derived from the cerulein-treated pancreas relative to controls and were further increased after halofuginone treatment. Equal levels of phosphorylated Akt and p38 MAPK were observed in PSCs derived from control and cerulein-treated mice and were unaltered after halofuginone treatment.

Halofuginone Affects Cerulein-Dependent Acinar Cell Proliferation and PAP-1 Synthesis

Fully differentiated pancreatic acinar cells are capable of replication and can reenter the cell cycle to restore lost acinar tissue.[44] Only a small number of PCNA-positive acinar cells were detected in the untreated pancreas, whereas after cerulein treatment, a major increase in PCNA-positive cells was observed (Fig. 6). Halofuginone prevented this increase only in the early stages of pancreas fibrosis development. In pathologic situations, the acinar cells are the main source of PAP-1.[33] Almost no PAP-1 was synthesized by the control untreated pancreas or by the pancreas of mice treated with halofuginone alone. Cerulein caused increased PAP-1 synthesis, which was more evident after 4 weeks of treatment, and halofuginone caused a further increase in this synthesis (Fig. 7).

DISCUSSION

Chronic pancreatitis is characterized by pancreatic inflammation and fibrosis, eventually leading to destruction of pancreatic parenchyma and loss of exocrine and endocrine functions. In response to pancreatic injury or inflammation, PSCs are activated into highly proliferative myofibroblastlike cells that express smooth muscle proteins and produce ECM components. Administration of cerulein caused a major increase in the synthesis of fibrosis-related and TGFβ-dependent proteins such as collagen type I and P4Hβ (Fig. 1), consistent with other models of pancreatitis.[34,35] Halofuginone inhibited PSC activation, in agreement with previous observations of inhibition of HSC and tumor myofibroblast activation,[20,22,23] as evidenced by the following findings. (1) There was inhibition of synthesis of collagen type I, the major ECM protein, and of P4Hβ, the main enzyme responsible for its cross-linking (Fig. 1). The Sirius red staining that remained after halofuginone treatment may partly represent collagen type III, which also increases in pancreas fibrosis[35] but is not affected by halofuginone.[36] Halofuginone also inhibited collagen synthesis in severe hyperstimulation and obstruction pancreatitis in rats.[37] (2) There was inhibition of the expression of specific markers expressed in activated PSCs, such as Cygb/STAP, and of TGFβ-dependent increases in muscle-specific genes such as SM22α (Figs. 2A, B). (3) There was inhibition of PSC proliferation (Fig. 2C). All of the inhibited parameters are characteristic of activated PSCs. Transforming growth factor β is known to regulate PSC activation and to inhibit its proliferation. Although halofuginone inhibited TGFβ signaling, incubation of the PSC with halofuginone resulted in a dose-dependent inhibition of cell proliferation (Fig. 2C). These results suggest that halofuginone may have additional targets involved in cell proliferation, for example, within the MAPK signaling pathway (Fig. 5).

The course of chronic pancreatitis is characterized by recurrent episodes of acute pancreatitis, which cause parenchymal injury and necrosis, accompanied by fibrosis, chronic inflammation, and parenchymal cell loss, all of which increase with each successive episode. Hypoxia and hypoxia-related genes are upregulated during cerulein-induced acute pancreatitis.[38] It is interesting to note that the synthesis of Cygb/STAP and collagen P4Hβ is controlled by hypoxia.[39,40] Cytoglobin/stellate cell activation–associated protein is probably involved in cellular oxygen homeostasis and supply and plays a role as an oxygen reservoir that is used under hypoxic conditions to protect the tissue from oxidative stress.[41]

Regardless of the cause of the insult resulting in pancreas fibrosis, extensive ECM remodeling is required. In the first

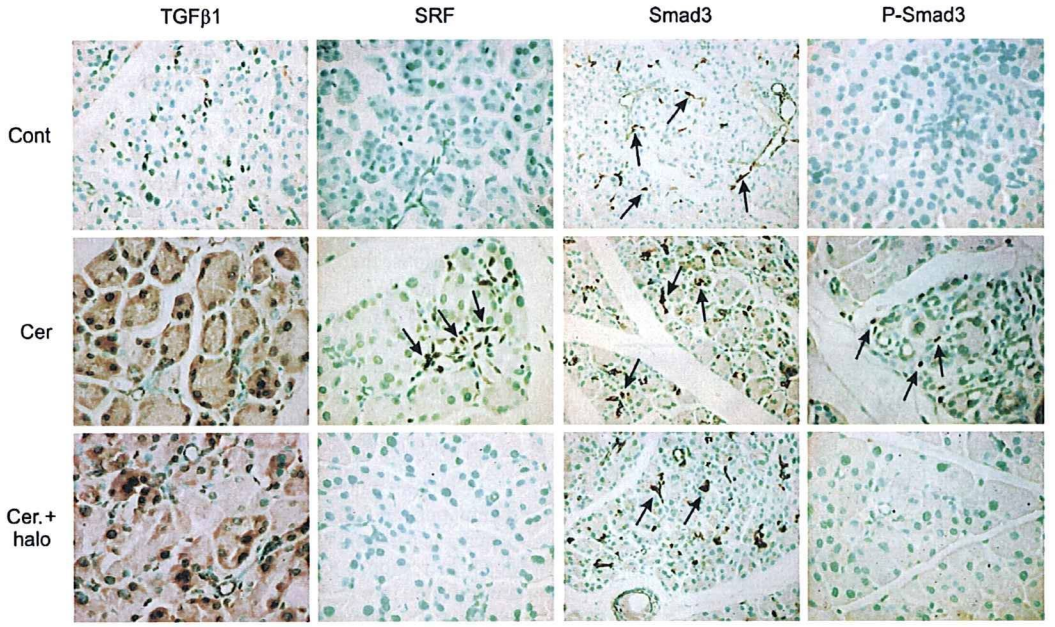

FIGURE 4. Halofuginone and TGFβ signaling. Transforming growth factor β, SRF, Smad3, and P-Smad3 levels were determined by immunohistochemistry in pancreas biopsies after 8 weeks of cerulein treatment, with or without halofuginone. Cells expressing the specific proteins are indicated by arrows. Note that halofuginone did not affect TGFβ levels but prevented the cerulein-dependent increases in SRF and P-Smad3, but not Smad3, levels.

step, transient local degradation of the ECM occurs, either by proteases of the plasminogen or by the MMP systems. The balance between the MMPs and their inhibitors is pivotal in the remodeling of the ECM. Tissue inhibitors of MMP-1 and TIMP2, derived from the activated PSCs,[16] are increased in the pancreas of cerulein-treated mice (Fig. 3A). Although both TIMPs are under the control of TGFβ, the regulation of TIMP1 is probably not Smad3-dependent. The Smad-containing complexes do not interact with the promoter-proximal activator protein 1 site of TIMP1 that is required for TGFβ activation; therefore, TGFβ was able to stimulate TIMP1 synthesis in a Smad-knockout cell line.[42] This could explain the observation that halofuginone, an inhibitor of Smad3 phosphorylation downstream of TGFβ signaling[21,23] (Fig. 4), inhibited only the synthesis of TIMP2 but not that of TIMP1 (Fig. 3A), as has been observed in chemically induced liver fibrosis.[20] Pancreatic stellate cells have the capacity to synthesize a number of MMPs under the control of TGFβ.[16] The PSCs derived from cerulein-treated mice exhibited much higher MMP-2 activity than those derived from the control mice, and the difference persisted even after several passages in culture (Fig. 3C). This may imply a fundamental genomic change while they are in the fibrotic tissue, or it may reflect the disparity in their origin. Halofuginone prevented the TGFβ-dependent increase in MMP-2 activity in both cell populations (Fig. 3D), but it increased MMP-3 activity only in the cells derived from cerulein-treated mice. These results are consistent with the effects of halofuginone on MMP activity observed in HSCs in culture and in rat hepatic-induced fibrosis.[43]

Transforming growth factor β is synthesized by the PSCs and was upregulated in the cerulein-treated pancreas (Fig. 4). Halofuginone, which has been found to overcome TGFβ-induced collagen synthesis without affecting TGFβ receptor expression,[23] did not affect TGFβ levels in the cerulein-treated mice, suggesting that halofuginone's target is probably downstream of the TGFβ-receptor interaction, along the Smad3 pathway. Indeed, halofuginone decreased the levels of P-Smad2/3 in the cerulein-treated pancreas without affecting the total level of Smad3, in agreement with previous findings.[21,23] Smad3, in conjunction with SRF, is a major mediator of TGFβ signaling, which results in transcription of smooth muscle–specific genes.[11] Serum response factor induces smooth muscle cell (SMC) gene expression, and the dominant-negative mutant of SRF blocks TGFβ-induced SMC genes.[44] In activated HSCs, TGFβ upregulates SRF synthesis, resulting in SMC gene expression.[45] The entire conditional inactivation of the SRF gene in the pancreas leads to severe pancreatitis,[46] although in the present study, in the cerulein-treated pancreas, SRF was upregulated exclusively by the PSCs, probably because of cerulein-dependent increases in TGFβ synthesis and Smad3 phosphorylation (Fig. 4). Halofuginone inhibited SRF synthesis without affecting the level of TGFβ, which again suggests that halofuginone inhibits smooth muscle gene expression and ECM production by inhibiting Smad3 phosphorylation downstream of TGFβ signaling, resulting in inhibition of PSC activation.

The PSCs derived from the pancreas of cerulein-treated mice exhibited much higher levels of phosphorylated JNK and, to a lesser extent, of MAPK/ERK, but not of p38 kinase or Akt. Halofuginone further increased JNK phosphorylation in the cerulein-treated PSCs. The JNK has been implicated as a repressor of TGFβ gene expression, and it contributes to the regulation of autocrine TGFβ-mediated biologic responses,[47] suggesting that there is cross-talk between the 2 signaling pathways. It is interesting to note that halofuginone causes increased phosphorylation of c-Jun transcription factor, a major JNK substrate, in Tsk/+ mouse fibroblasts in culture and in vivo, in correlation with a decrease in collagen synthesis.[48]

Halofuginone affects not only the stellate cells but also the epithelial cells of the tissue. In the liver, halofuginone stimulates insulin growth factor binding protein 1 synthesis by the hepatocytes, and the secreted insulin growth factor binding

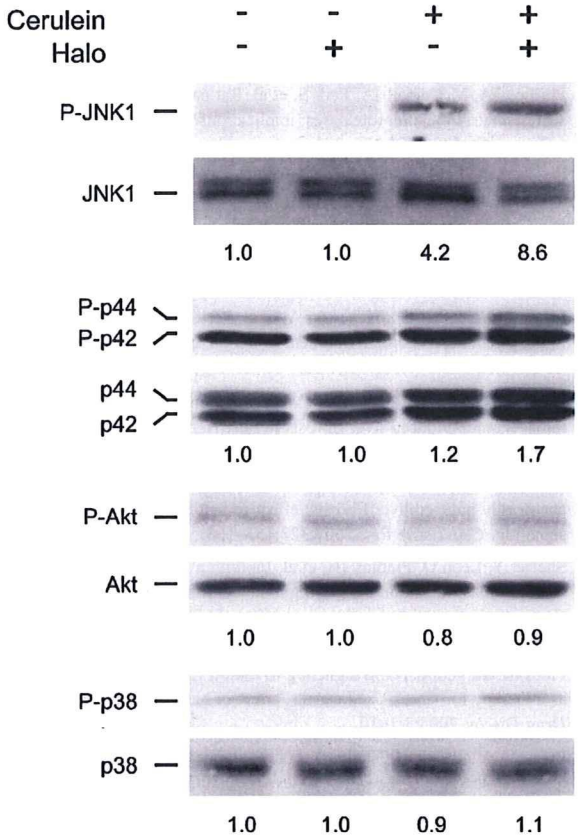

FIGURE 5. Halofuginone and JNK, MAPK, and Akt signaling in PSCs. Cells derived from the pancreas of control and cerulein-treated mice were cultured in the presence or absence of halofuginone (20 mmol/L). At the end of the incubation, cell extracts were blotted with the appropriate antibodies. Halofuginone further increased the cerulein-dependent phosphorylation of JNK and, to a lesser extent, the phosphorylation of MAPK/ERK. No effect of cerulein or halofuginone on Akt or p38 phosphorylation was observed.

protein 1 inhibits HSC migration.[27] In the pancreas, PAP-1 is expressed at a level related to the severity of cerulein-induced pancreatitis in the acute phase.[49] Halofuginone prevented the

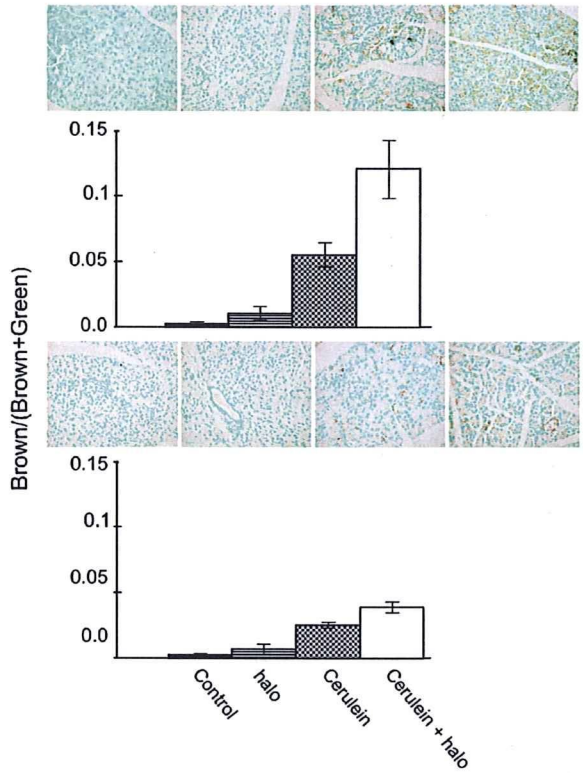

FIGURE 7. Halofuginone and PAP-1 synthesis. Pancreas biopsies were taken after 4 and 8 weeks of cerulein treatment, with and without halofuginone, immunostained with PAP-1 antibodies, and subjected to image analysis. In each panel, means without a common letter differ significantly ($P < 0.05$) according to Duncan multiple range test.

cerulein-dependent increase in acinar cell proliferation and increased the synthesis of anti-inflammatory cytokine PAP-1 (Figs. 6, 7), which may further reduce PSC activation and matrix synthesis, by inhibiting inflammation. Halofuginone also inhibited rat inflammation after severe hyperstimulation and obstruction pancreatitis.[37]

In conclusion, we demonstrated that halofuginone prevents cerulein-dependent PSC activation by inhibiting Smad3

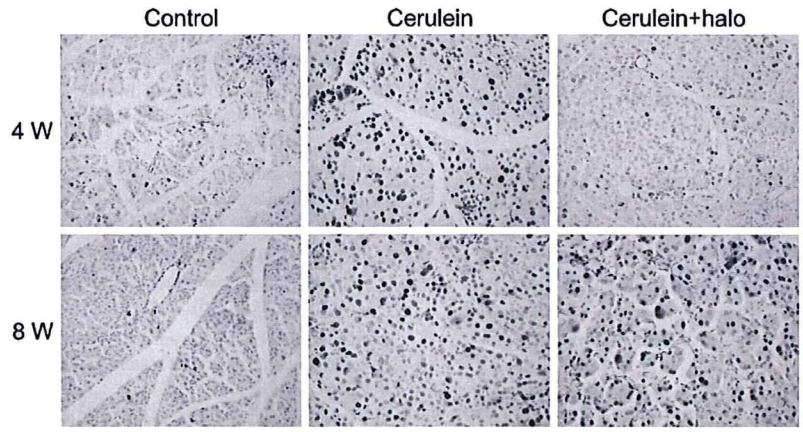

FIGURE 6. Halofuginone and acinar cell proliferation. Pancreas biopsies were taken after 4 and 8 weeks of cerulein treatment, with and without halofuginone, and were immunostained with PCNA antibodies. Halofuginone prevented the increase in acinar cell proliferation after only 4 weeks of treatment.

phosphorylation downstream of TGFβ signaling and via JNK phosphorylation. In addition, halofuginone increases the synthesis of the anti-inflammatory cytokine PAP-1 by the acinar cells, which can further reduce pancreas fibrosis. These results suggest that halofuginone, which has already exhibited human clinical efficacy[25,29] and is currently being evaluated in clinical trials for various indications,[50] could serve as a novel therapy for pancreas fibrosis.

ACKNOWLEDGMENT

This article is a contribution from the ARO, The Volcani Center.

REFERENCES

1. Witt H, Apte MV, Keim V, et al. Chronic pancreatitis: challenges and advances in pathogenesis, genetics, diagnosis, and therapy. *Gastroenterology.* 2007;132:1557–1573.
2. Kloppel G, Detlefsen S, Feyerabend B. Fibrosis of the pancreas: the initial tissue damage and the resulting pattern. *Virchows Arch.* 2004;445:1–8.
3. Apte MV, Wilson JS. Mechanisms of pancreatic fibrosis. *Dig Dis.* 2004;22:273–279.
4. Bachem MG, Schunemann M, Ramadani M, et al. Pancreatic carcinoma cells induce fibrosis by stimulating proliferation and matrix synthesis of stellate cells. *Gastroenterology.* 2005;128:907–921.
5. McCarroll JA, Phillips PA, Park S, et al. Pancreatic stellate cell activation by ethanol and acetaldehyde: is it mediated by the mitogen-activated protein kinase signaling pathway? *Pancreas.* 2003;27:150–160.
6. Nakatani K, Okuyama H, Shimahara Y, et al. Cytoglobin/STAP, its unique localization in splanchnic fibroblast-like cells and function in organ fibrogenesis. *Lab Invest.* 2004;84:91–101.
7. Apte MV, Phillips PA, Fahmy RG, et al. Does alcohol directly stimulate pancreatic fibrogenesis? Studies with rat pancreatic stellate cells. *Gastroenterology.* 2000;118:780–794.
8. Luttenberger T, Schmid-Kotsas A, Menke A, et al. Platelet-derived growth factors stimulate proliferation and extracellular matrix synthesis of pancreatic stellate cells: implications in pathogenesis of pancreas fibrosis. *Lab Invest.* 2000;80:47–55.
9. Yoo BM, Yeo M, Oh TY, et al. Amelioration of pancreatic fibrosis in mice with defective TGF-beta signaling. *Pancreas.* 1995;30:71–79.
10. Roberts AB, Russo A, Felici A, et al. Smad3: a key player in pathogenetic mechanisms dependent on TGF-beta. *Ann N Y Acad Sci.* 2003;995:1–10.
11. Qiu P, Feng XH, Li L. Interaction of Smad3 and SRF-associated complex mediates TGF-beta1 signals to regulate SM22 transcription during myofibroblast differentiation. *J Mol Cell Cardiol.* 2003;35:1407–1420.
12. Mack CP, Thompson MM, Lawrenz-Smith S, et al. Smooth muscle alpha-actin CArG elements coordinate formation of a smooth muscle cell–selective, serum response factor–containing activation complex. *Circ Res.* 2000;86:221–232.
13. Jesnowski R, Furst D, Ringel J, et al. Immortalization of pancreatic stellate cells as an in vitro model of pancreatic fibrosis: deactivation is induced by matrigel and *N*-acetylcysteine. *Lab Invest.* 2005;85: 1276–1291.
14. Ishihara T, Hayasaka A, Yamaguchi T, et al. Immunohistochemical study of transforming growth factor-beta 1, matrix metalloproteinase-2,9, tissue inhibitors of metalloproteinase-1,2, and basement membrane components at pancreatic ducts in chronic pancreatitis. *Pancreas.* 1998;17:412–418.
15. Yokota T, Denham W, Murayama K, et al. Pancreatic stellate cell activation and MMP production in experimental pancreatic fibrosis. *J Surg Res.* 2002;104:106–111.
16. Phillips PA, McCarroll JA, Park S, et al. Rat pancreatic stellate cells secrete matrix metalloproteinases: implications for extracellular matrix turnover. *Gut.* 2003;52:275–282.
17. Omary MB, Lugea A, Lowe AW, et al. The pancreatic stellate cell: a star on the rise in pancreatic diseases. *J Clin Invest.* 2007;117:50–59.
18. Hwang RF, Moore T, Arumugam T, et al. Cancer-associated stromal fibroblasts promote pancreatic tumor progression. *Cancer Res.* 2008;68:918–926.
19. Erkan M, Kleeff J, Gorbachevski A, et al. Periostin creates a tumor-supportive microenvironment in the pancreas by sustaining fibrogenic stellate cell activity. *Gastroenterology.* 2007;132:1447–1464.
20. Bruck R, Genina O, Aeed H, et al. Halofuginone to prevent and treat thioacetamide-induced liver fibrosis in rats. *Hepatology.* 2001;3: 379–386.
21. Gnainsky Y, Kushnirsky Z, Bilu G, et al. Gene expression during chemically induced liver fibrosis: effect of halofuginone on TGF-beta signaling. *Cell Tissue Res.* 2007;328:153–166.
22. Sheffer Y, Leon O, Pinthus JH, et al. Inhibition of fibroblast to myofibroblast transition by halofuginone contributes to the chemotherapy-mediated antitumoral effect. *Mol Cancer Ther.* 2007;6: 570–577.
23. Pines M. Targeting TGFβ signaling to inhibit fibroblast activation as a therapy for fibrosis and cancer: effect of halofuginone. *Exp Opion Drug Discov.* 2008;3:1–10.
24. Pines M, Vlodavsky I, Nagler A. Halofuginone: from veterinary use to human therapy. *Drug Develop Res.* 2000;50:371–378.
25. Pines M, Snyder D, Yarkoni S, et al. Halofuginone to treat fibrosis in chronic graft versus host disease and scleroderma. *Biol Bl Marrow Transplant.* 2003;9:417–425.
26. Spira G, Mawasi N, Paizi M, et al. Halofuginone, a collagen type I inhibitor improves liver regeneration in cirrhotic rats. *J Hepatol.* 2002;37:331–339.
27. Gnainsky Y, Spira G, Paizi M, et al. Halofuginone—an inhibitor of collagen synthesis by rat stellate cells—stimulates insulin-like growth factor-binding protein 1 synthesis by hepatocytes. *J Hepatol.* 2003;40: 269–277.
28. Gnainsky Y, Spira G, Paizi M, et al. The involvement of the tyrosine phosphatase early gene of liver regeneration (PRL-1) in cell cycle and in liver regeneration and fibrosis—effect of halofuginone. *Cell Tissue Res.* 2006;324:385–394.
29. Nagler A, Pines M. Topical treatment of cutaneous chronic graft versus host disease (cGvHD) with halofuginone: a novel inhibitor of collagen type I synthesis. *Transplantation.* 1999;68:1806–1809.
30. Keim V, Iovanna JL, Orelle B, et al. A novel exocrine protein associated with pancreas transplantation in humans. *Gastroenterology.* 1992;103:248–254.
31. Neuschwander-Tetri BA, Burton FR, Presti ME, et al. Repetitive self-limited acute pancreatitis induces pancreatic fibrogenesis in the mouse. *Dig Dis Sci.* 2000;45:665–674.
32. Kruse ML, Hildebrand PB, Timke C, et al. Isolation, long-term culture, and characterization of rat pancreatic fibroblastoid/stellate cells. *Pancreas.* 2001;23:49–54.
33. Closa D, Motoo Y, Iovanna JL. Pancreatitis-associated protein: from a lectin to an anti-inflammatory cytokine. *World J Gastroenterol.* 2007;13:170–174.
34. Koslowski R, Seidel D, Kuhlisch E, et al. Evidence for the involvement of TGF-beta and PDGF in the regulation of prolyl 4-hydroxylase and lysyloxidase in cultured rat lung fibroblasts. *Exp Toxicol Pathol.* 2003;55:257–264.

35. Miyauchi M, Suda K, Kuwayama C, et al. Role of fibrosis-related genes and pancreatic duct obstruction in rat pancreatitis models: implications for chronic pancreatitis. *Histol Histopathol.* 2007;22:1119–1127.
36. Choi ET, Callow AD, Sehgal NL, et al. Halofuginone, a specific collagen type I inhibitor, reduces anastomotic intimal hyperplasia. *Arch Surg.* 1995;130:257–261.
37. Karatas A, Paksoy M, Erzin Y, et al. The effect of halofuginone, a specific inhibitor of collagen type 1 synthesis, in the prevention of pancreatic fibrosis in an experimental model of severe hyperstimulation and obstruction pancreatitis. *J Surg Res.* 2008;148:7–12.
38. Gomez G, Englander EW, Wang G, et al. Increased expression of hypoxia-inducible factor-1alpha, p48, and the Notch signaling cascade during acute pancreatitis in mice. *Pancreas.* 2004;28:58–64.
39. Fähling M, Perlewitz A, Doller A, et al. Regulation of collagen prolyl 4-hydroxylase and matrix metalloproteinases in fibrosarcoma cells by hypoxia. *Comp Biochem Physiol C Toxicol Pharmacol.* 2004;139:119–126.
40. Fordel E, Thijs L, Martinet W, et al. Anoxia or oxygen and glucose deprivation in SH-SY5Y cells: a step closer to the unraveling of neuroglobin and cytoglobin functions. *Gene.* 2007;398:114–122.
41. Xu R, Harrison PM, Chen M, et al. Cytoglobin overexpression protects against damage-induced fibrosis. *Mol Ther.* 2006;13:1093–1100.
42. Hall MC, Young DA, Waters JG, et al. The comparative role of activator protein 1 and Smad factors in the regulation of Timp-1 and MMP-1 gene expression by transforming growth factor-beta 1. *J Biol Chem.* 2003;278:10304–10313.
43. Popov Y, Patsenker E, Bauer M, et al. Halofuginone induces matrix metalloproteinases in rat hepatic stellate cells via activation of p38 and NFkappaB. *J Biol Chem.* 2006;281:15090–15098.
44. Hirschi KK, Lai L, Belaguli NS, et al. Transforming growth factor-beta induction of smooth muscle cell phenotype requires transcriptional and post-transcriptional control of serum response factor. *J Biol Chem.* 2002;277:6287–6295.
45. Herrmann J, Haas U, Gressner AM, et al. TGF-beta up-regulates serum response factor in activated hepatic stellate cells. *Biochim Biophys Acta.* 2007;1772:1250–1257.
46. Miralles F, Hebrard S, Lamotte L, et al. Conditional inactivation of the murine serum response factor in the pancreas leads to severe pancreatitis. *Lab Invest.* 2006;86:1020–1036.
47. Ventura JJ, Kennedy NJ, Flavell RA, et al. JNK regulates autocrine expression of TGF-beta1. *Mol Cell.* 2004;15:269–278.
48. McGaha TL, Kodera T, Spiera H, et al. Halofuginone inhibition of COL1A2 promoter activity via a c-Jun–dependent mechanism. *Arthritis Rheum.* 2002;46:2748–2761.
49. Magaña-Gómez J, López-Cervantes G, Calderón de la Barca AM. Caerulin-induced pancreatitis in rats: histological and genetic expression changes from acute phase to recuperation. *World J Gastroenterol.* 2006;12:3999–4003.
50. de Jonge MJ, Dumez H, Verweij J, et al. EORTC New Drug Development Group (NDDG). Phase I and pharmacokinetic study of halofuginone, an oral quinazolinone derivative in patients with advanced solid tumours. *Eur J Cancer.* 2006;42:1768–1774.

Chem. Res. Toxicol. **2010,** *23,* 152–158

Approach for *in Vivo* Protein Binding of 5-*n*-Butyl-pyrazolo[1,5-*a*]pyrimidine Bioactivated in Chimeric Mice with Humanized Liver by Two-Dimensional Electrophoresis with Accelerator Mass Spectrometry

Hiroshi Yamazaki,*,† Shunji Kuribayashi,‡ Tae Inoue,§,|| Chise Tateno,§ Yasufumi Nishikura,§ Ken Oofusa,⊥ Daisuke Harada,‡ Shinsaku Naito,‡ Toru Horie,§ and Shigeru Ohta||

Showa Pharmaceutical University, Machida, Tokyo 194-8543, Japan, Preclinical Assessment Department, Otsuka Pharmaceutical Factory, Inc., Naruto, Tokushima 772-8601, Japan, PhoenixBio, Co., Higashi-Hiroshima, Hiroshima 739-0046, Japan, Graduate School of Biomedical Sciences, Hiroshima University, Minami-ku, Hiroshima 734-8553, Japan, and Towa Environment Science Co., Suminoe-ku, Osaka 559-0034, Japan

Received September 9, 2009

Drug development of a potential analgesic agent 5-*n*-butyl-7-(3,4,5-trimethoxybenzoylamino)pyrazolo[1,5-*a*]pyrimidine was withdrawn because of its limited hepatotoxic effects in humans that could not be predicted from regulatory animal or *in vitro* studies. *In vivo* formation of glutathione conjugates and covalent binding of a model compound 5-*n*-butyl-pyrazolo[1,5-*a*]pyrimidine were investigated in the present study after intravenous administration to chimeric mice with a human or rat liver because of an interesting capability of human cytochrome P450 1A2 in forming a covalently bound metabolite *in vitro*. Rapid distribution and elimination of radiolabeled 5-*n*-butyl-pyrazolo[1,5-*a*]pyrimidine in plasma or liver fractions were seen in chimeric mice after intravenous administration. However, similar covalent binding in liver was detected over 0.17−24 h after intravenous administration. Radio-LC analyses revealed that the chimeric mice with humanized liver preferentially gave the 3-hydroxylated metabolite and its glutathione conjugate in the plasma and liver. On the contrary, chimeric mice with a rat liver had some rat-specific metabolites *in vivo*. Analyses by electrophoresis with accelerator mass spectrometry of *in vivo* radiolabeled liver proteins in chimeric mice revealed that bioactivated 5-*n*-butyl-pyrazolo[1,5-*a*]-pyrimidine bound nonspecifically to a variety of microsomal proteins including human P450 1A2 as well as cytosolic proteins in the livers from chimeric mice with humanized liver. These results suggest that the hepatotoxic model compound 5-*n*-butyl-pyrazolo[1,5-*a*]pyrimidine was activated by human liver microsomal P450 1A2 to reactive intermediate(s) *in vivo* in humanized chimeric mice and could relatively nonspecifically bind to biomolecules such as P450 1A2 and other proteins.

Introduction

Cytochrome P450 comprises a superfamily of enzymes involved in the oxidation of a large number of endogenous and exogenous compounds associated with their pharmacological or toxicological actions (*1*). For example, it has been reported that drug-induced hepatotoxicity may be caused by active intermediates formed by animal and/or human P450 enzymes from a common toxicant acetaminophen (*2*) or idiosyncratic troglitazone withdrawn from the market (*3*). Species differences between experimental animals and humans in the roles of P450 enzymes in drug metabolism are determinant factors in evaluating drug toxicity (*4*).

Drug-induced liver injury has been one of the most frequent single causes of safety-related drug marketing withdrawals. In a clinical study of 5-*n*-butyl-7-(3,4,5-trimethoxybenzoylamino)pyrazolo[1,5-*a*]pyrimidine (Figure 1, OT-7100[1]) with a potential analgesic effect, limited elevations in the serum levels of asparate or alanine aminotransferase were abnormally observed in humans that could not be predicted from regulatory animal or *in vitro* studies (*5*). No apparent differences in plasma drug levels of volunteers were found between the toxic cases and other groups in our limited observations so far (*5*). The underlying molecular mechanisms are not yet fully known. However, human liver microsomal P450 1A2 was able to effectively mediate the transformation of a primary metabolite 5-*n*-butyl-pyrazolo[1,5-*a*]pyrimidine (M-5) into 3-hydroxy-5-*n*-butyl-pyrazolo[1,5-*a*]pyrimidine (M-23OH), yielding a possible quinone-imine metabolite that could bind to glutathione or liver proteins (Figure 1) (*5*).

Safety assessment of drug metabolites is proposed by potential application of genetically engineered mouse models that express human P450 enzymes (*6*). Recently, chimeric mice with humanized liver were established by transplanting human hepatocytes into a urokinase-type plasminogen activator$^{+/+}$/

* Corresponding author. Showa Pharmaceutical University, 3-3165 Higashi-tamagawa Gakuen, Machida, Tokyo 194-8543, Japan. Tel/Fax: +81-42-721-1406. E-mail: hyamazak@ac.shoyaku.ac.jp.
† Showa Pharmaceutical University.
‡ Otsuka Pharmaceutical Factory, Inc.
§ PhoenixBio Co.
|| Hiroshima University.
⊥ Towa Environment Science Co.

[1] Abbreviations: M-5, 5-*n*-butyl-pyrazolo[1,5-*a*]pyrimidine; M-22OH, 6-hydroxy-5-*n*-butyl-pyrazolo[1,5-*a*]pyrimidine; M-23OH, 3-hydroxy-5-*n*-butyl-pyrazolo[1,5-*a*]pyrimidine; OT-7100, 5-*n*-butyl-7-(3,4,5-trimethoxybenzoylamino)pyrazolo[1,5-*a*]pyrimidine.

10.1021/tx900323a
Published on Web 11/24/2009

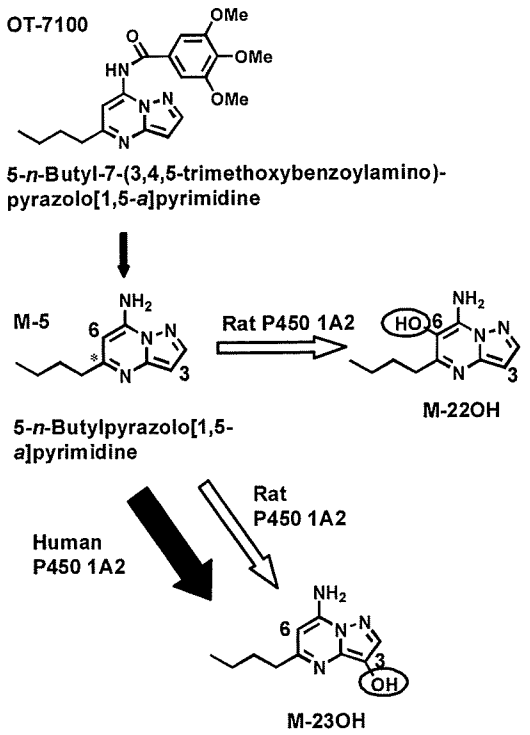

Figure 1. Metabolic fate of human hepatotoxic pyrazolopyrimidine derivative, 5-*n*-butyl-7-(3,4,5-trimethoxybenzoylamino)pyrazolo[1,5-*a*]-pyrimidine (OT-7100) and its primary metabolite 5-*n*-butyl-pyrazolo[1,5-*a*]pyrimidine (M-5), after biotransformation by human and rat P450 1A2 enzymes. Only 3-hydroxy-5-*n*-butyl-pyrazolo[1,5-*a*]pyrimidine (M-23OH) was detected in human liver microsomal incubations, but M-23OH and hydroxy-5-*n*-butyl-pyrazolo[1,5-*a*]pyrimidine (M-22OH) were seen in rat liver microsomal incubations (*5*).

severe combined immunodeficient transgenic mouse line (*7, 8*). These chimeric mice may be useful to evaluate human pharmacokinetics for developing drug candidates or idiosyncratic drugs in terms of mechanism-based adverse reactions and toxicity.

The purpose of this study was to characterize *in vivo* 5-*n*-butyl-pyrazolo[1,5-*a*]pyrimidine metabolism by human liver microsomal P450 enzymes transplanted into mice and also to better understand the activation of 5-*n*-butyl-pyrazolo[1,5-*a*]-pyrimidine and any interactions with biomolecules in the liver including covalent binding by electrophoresis analysis with accelerator mass spectrometry. In order to investigate different oxidative metabolic profiles of the species-specific hepatotoxic pyrazolopyrimidine derivative, chimeric mice with rat livers (*7, 9*) were also used and compared with mice with humanized livers. We report herein that the metabolically activated 5-*n*-butyl-pyrazolo[1,5-*a*]pyrimidine binds nonspecifically to a variety of microsomal proteins including human P450 1A2 (a bioactivating enzyme) or prolyl-4-hydroxylase as well as cytosolic proteins including catalase in chimeric mice with humanized livers.

Experimental Procedures

Chemicals and Enzymes. 5-*n*-Butyl-pyrazolo[1,5-*a*]pyrimidine (M-5) and its ^{14}C-labeled compound (the labeling position was the 5 position carbon atom in the pyrazolopyrimidine ring as shown in Figure 1), 3-hydroxy-5-*n*-butyl-pyrazolo[1,5-*a*]pyrimidine (M-23OH), 6-hydroxy-5-*n*-butyl-pyrazolo[1,5-*a*]pyrimidine (M-22OH), and 5-*n*-pentyl-7-(3,4,5-trimethoxybenzoylamino)pyrazolo[1,5-*a*] pyrimidine (OT-7126) as an internal standard for HPLC analysis were synthesized at Otsuka Pharmaceutical Factory (Tokushima, Japan). All these chemicals were determined, by reversed-phase HPLC, to be >99.0% pure. Reduced glutathione was purchased from Sigma-Aldrich (St. Louis, MO). Recombinant human and rat P450 1A2 coexpressed with NADPH-P450 reductase in baculovirus-infected insect cells (Supersomes) and antibodies against human P450 enzymes were purchased from Nosan (Yokohama, Japan) and BD Gentest (Woburn, MA). All other chemicals and reagents used were of analytical reagent grade.

Animal Experiments. Chimeric mice (PXB mice) with a human or rat liver used in this study were prepared by PhoenixBio Co. (Hiroshima, Japan) (*7, 9*). Briefly, male chimeric mice (10−14 weeks old, 15 g body weight) with human hepatocytes (male Caucasian, 2 years old from BD Biosciences, San Jose, CA) or rat hepatocytes (pooled from five male Sprague−Dawley rats, 10 weeks old were purchased from Charles River Japan, Kanagawa, Japan) were transplanted into a urokinase-type plasminogen activator $^{+/+}$/severe combined immunodeficient transgenic mouse line (20−30 days after birth). The replacement index of the mice with the human hepatocytes for estimating the humanization of the chimeric mice was determined by measuring the levels of human albumin in the mouse blood (*10*). The livers were collected and stored at −80 °C prior to use. The frozen tissues were homogenized with 5 volume of 250 mM sucrose buffer. Protein concentrations of these samples were measured by a protein assay system (Bio-Rad Laboratories, Hercules, CA).

Metabolites Measurements. A typical *in vitro* incubation mixture (0.50 mL total volume) contained recombinant human or rat P450 1A2 (20 pmol equivalent recombinant P450/mL), 50 mM potassium phosphate buffer (pH 7.4), an NADPH-generating system (0.5 mM $NADP^+$, 5 mM glucose 6-phosphate, and 1 U/mL glucose-6-phosphate dehydrogenase), and 5-*n*-butyl-pyrazolo[1,5-*a*]pyrimidine (5.0 μM) in the absence or presence of reduced glutathione (50 mM). After a 5 min preincubation, the reactions were initiated by the addition of the NADPH-generating system and were incubated at 37 °C for 30 min. The reactions were terminated by 0.50 mL of methanol, and then OT-7126 was added as an internal standard. After centrifugation at 2,000*g* for 10 min at 4 °C, the supernatant was added to 5 mM ammonium acetate at a ratio of 1:1, and a 0.20 mL aliquot was injected onto the LC system. In the case of the analysis of *in vivo* samples, a 0.2 mL aliquot of each plasma or liver homogenate sample was first added to 0.46 mL of methanol, and then OT-7126 was added as an internal standard. After centrifugation at 10,000*g* for 15 min at 4 °C, the supernatant (0.5 mL) was transferred to another tube and dried under nitrogen at 40 °C. The residue was dissolved in 0.2 mL of a mixture of methanol and 5 mM ammonium acetate at a ratio of 1:3, and a 0.15 mL aliquot was injected onto the radio-LC system.

HPLC Analysis. 5-*n*-Butyl-pyrazolo[1,5-*a*]pyrimidine and its metabolites were assayed using UV-LC and radio-LC methods validated over a concentration range of 0.10−10.0 μM. 5-*n*-Butyl-pyrazolo[1,5-*a*]pyrimidine and its metabolites in incubation mixtures or plasma and liver homogenates of the chimeric mice were separated on a 250 mm × 4.6 mm i.d. Inertsil ODS-3 V column (GL-Sciences, Tokyo, Japan) and detected at wavelengths of 230 nm or by FLO-ONE/Beta Model A525 as a radio-detector using an HPLC system (LC-10A Series, Shimadzu, Kyoto, Japan). The column temperature was maintained at 40 °C. The mobile phase was 5 mM ammonium acetate (A) and acetonitrile (B). The conditions for elution were as follows: 13 to 25% B (0−8 min), 25 to 25% B (8−20 min), 25 to 35% B (20−25 min), 35 to 80% B (25−31 min), and 80 to 80% B (31−40 min). Linear gradients were used for all solvent changes. The flow rate was 0.80 mL/min in LC assays in combination with the scintillator (Ultima-Flo, PerkinElmer, Waltham, MA, at a flow rate of 2.4 mL/min) in the radio-LC assay.

Covalent Binding of Metabolically Activated Derivatives to the Liver *in Vivo*. A sodium dodecyl sulfate (SDS)−polyacrylamide gel electrophoretogram in 12% acrylamide gels with liver microsomes (10 μg) from humanized mice treated with 5-*n*-butyl-pyrazolo[1,5-*a*]pyrimidine (*5, 11*) was stained with 0.08% Coomassie Brilliant Blue R350 (GE Healthcare Bio-Science) according to the manufacturer's protocol. Radioactivity contents of each band

on the gel were determined by BAS-5000 Image Analysis System (Fujifilm, Tokyo, Japan). In separate experiments, 10 gel pieces were sliced-out by hand at 1 mm width at 35−100 kDa range from the gel after electrophoresis and were subjected to mass spectrometry for detecting P450 enzymes. In other experiments, corresponding human P450 enzymes in liver microsomes separated on the gel were also detected with anti-P450 antibodies.

Protein samples (100 μg) were applied overnight to Immobiline Drystrip (GE Healthcare Bio-Science) by in-gel rehydration as described previously (*12, 13*). After rehydrated gels were gently dried, isoelectric focusing was performed in a Pharmacia Hoefer Multiphor II electrophoresis chamber (GE Healthcare, Buckinghamshire, U.K.) according to the manufacturer's instructions. Second dimension SDS−polyacrylamide gel electrophoresis (PAGE) was performed in 9−18% acrylamide gradient gels using a IsoDalt electrophoresis chamber. The second dimension gels were stained with SYPRO Ruby (Invitrogen, Carlsbad, CA) under the manufacturer's protocols (*14*). The SYPRO Ruby-stained proteins were detected using Molecular Imager FX (Bio-Rad Laboratories, Hercules, CA) and were subjected to in-gel digestion image analysis. Database management and image analysis were done using Image Master Platinum image analysis software (GE Healthcare).

In-gel digestion and mass spectrometric identification of proteins were performed essentially as described elsewhere (*15*). Briefly, protein spots were excised from the dried silver stained second dimension gels and rehydrated for 20 min in 100 mM NH_4HCO_3. The gel spots were then destained for 20 min in a solution of 15 mM potassium ferricyanide and 50 mM thiosulfate (*16*), rinsed twice in water, and finally dehydrated in 100% acetonitrile until they turned opaque white. The spots were then dried in a vacuum centrifuge and subsequently rehydrated in a digestion solution consisting of 50 mM NH_4HCO_3, 5 mM $CaCl_2$, and 0.1 μg/μL modified sequence-grade trypsin (Promega, Madison, WI). After overnight incubation at 37 °C, the digestion was terminated in 5% trifluoroacetic acid for 20 min. Peptides were extracted 3 times (20 min each) with 5% trifluoroacetic acid in 50% acetonitrile, and the extracted peptides were pooled and dried in a vacuum centrifuge. The peptides were purified with ZipTip (Millipore, Billerica, MA) under the manufacturer's protocol and analyzed by MACOT database software (Matrix Science, Tokyo, Japan). Accelerator mass spectrometry analyses were performed with a NEC 1.5SDH-1 0.6MV Pelletron AMS system (National Electrostatics Corporation, Tokyo, Japan) to determine $^{14}C/^{12}C$ content ratio in the biological samples after dilution as described previously (*17*).

Kinetic Data Analysis. The radioactive concentrations at time 0 (C_0) were extrapolated from the initial slope. The times to reach the elimination half-lives ($t_{1/2}$) were estimated as ln 2/k, where k is the slope of the terminal linear portion of the semilogarithmic plasma concentration−time curve. The areas under the plasma concentration−time curves from time 0 to the last detectable concentration ($AUC_{0\text{-}t}$), area under the plasma concentration−time curves from time 0 to the infinite time after administration ($AUC_{0\text{-}\infty}$), and the mean residence times (MRT) were calculated. Total systemic clearances (CL_{tot}), volume of distribution (Vd), and volume of distribution at steady state ($Vdss$) were calculated according to the following equations: $CL_{tot} = D/AUC_{0\text{-}\infty}$, $Vd = D/C_0$, $Vdss = MRT{\cdot}CL_{tot} = D{\cdot}MRT/AUC_{0\text{-}\infty}$, where D is the administered dose.

Results

***In Vitro* Formation of Glutathione Conjugates of 5-*n*-Butyl-pyrazolo[1,5-*a*]pyrimidine Catalyzed by Recombinant Human or Rat P450 1A2.** Recombinant human or rat P450 1A2 was incubated with 5-*n*-butyl-pyrazolo[1,5-*a*]pyrimidine for 30 min with an NADPH-generating system and/or reduced glutathione (5.0 mM). Human P450 1A2 preferentially metabolized 5-*n*-butyl-pyrazolo[1,5-*a*]pyrimidine to M-23OH (peak 4, a C-3-position hydroxyl derivative) at substrate concentrations of 5.0 μM (Figure 2A). On the contrary, rat P450 1A2 rapidly metabolized 5-*n*-butyl-pyrazolo[1,5-*a*]pyrimidine to M-23OH, M-22OH (peak 3, a C-6-position hydroxyl derivative), or an unknown metabolite (peak 2, Figure 2C). An M-23OH-glutathione conjugate (peak 1) was also detected in the presence of glutathione and NADPH after the incubation of 5-*n*-butyl-pyrazolo[1,5-*a*]pyrimidine by P450 1A2 systems (Figure 2B,D).

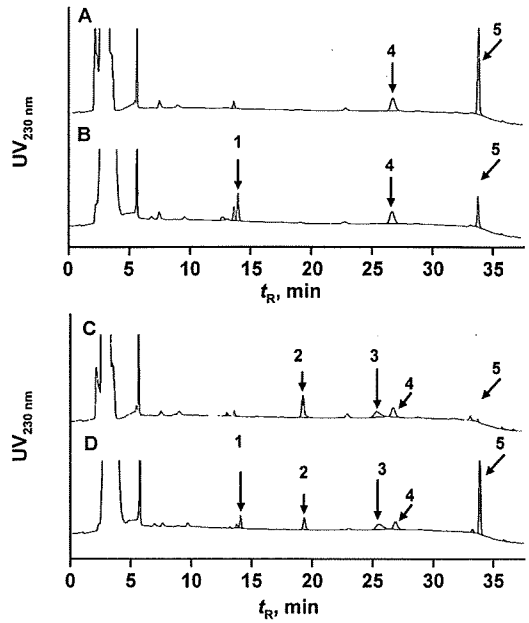

Figure 2. Representative UV-LC chromatograms of *in vitro* metabolites from 5-*n*-butyl-pyrazolo[1,5-*a*]pyrimidine (M-5) by incubation with human P450 1A2 (A,B) and rat P450 1A2 (C,D) in the absence (A,C) and presence (B,D) of reduced glutathione. Recombinant human or rat P450 1A2 (20 pmol/mL) was incubated with 5 μM 5-*n*-butyl-pyrazolo[1,5-*a*]pyrimidine (M-5) for 30 min with an NADPH-generating system and/or reduced glutathione (50 mM). Peak 1, a glutathione conjugate of M-23OH; peak 2, a rat-specific unknown product; peak 3, M-22OH; peak 4, M-23OH; and peak 5, 5-*n*-butyl-pyrazolo[1,5-*a*]-pyrimidine (M-5).

***In Vivo* Formation of Glutathione Conjugates of 5-*n*-Butyl-pyrazolo[1,5-*a*]pyrimidine after Intravenous Administration to Chimeric Mice with Human or Rat Livers.** To see *in vivo* species differences found in the 5-*n*-butyl-pyrazolo[1,5-*a*]pyrimidine metabolism *in vitro*, 5-*n*-butyl-pyrazolo[1,5-*a*]pyrimidine metabolism was investigated using chimeric mice with human or rat livers. After the administration of ^{14}C-5-*n*-butyl-pyrazolo[1,5-*a*]pyrimidine at 3 mg dose/kg body weight to chimeric mice, similar elimination curves of radioactivities in plasma were obtained in chimeric mice with a human and rat liver (Figure 3A). Similar elimination profiles were also seen in normal rats (not shown). The apparently similar pharmacokinetic parameters for radioactivity after intravenous administration of ^{14}C-5-*n*-butyl-pyrazolo[1,5-*a*]pyrimidine were obtained in chimeric mice with human or rat livers as shown in Table 1. The radioactivities were rapidly eliminated from the plasma of chimeric mice: half-lives of α- and β-elimination phases were 0.31 ± 0.06 h (mean ± SD) and 6.17 ± 1.28 h in chimeric mice with human livers. Similarly, rapid distribution (at 0.17 h after administration) and elimination (at 24 h) of radioactivity in liver fractions were seen in chimeric mice with human or rat livers after intravenous administration (Figure 3B). However, similar levels of covalent binding in livers were detected over 0.17−24 h both in chimeric mice with human and rat livers (Figure 3C).

Radio-LC assays revealed that the chimeric mice with human livers preferentially gave the M-23OH metabolite from 5-*n*-butyl-pyrazolo[1,5-*a*]pyrimidine in the liver (Figure 4C) and an M-23OH-glutathione conjugate in the plasma (Figures 4A). The

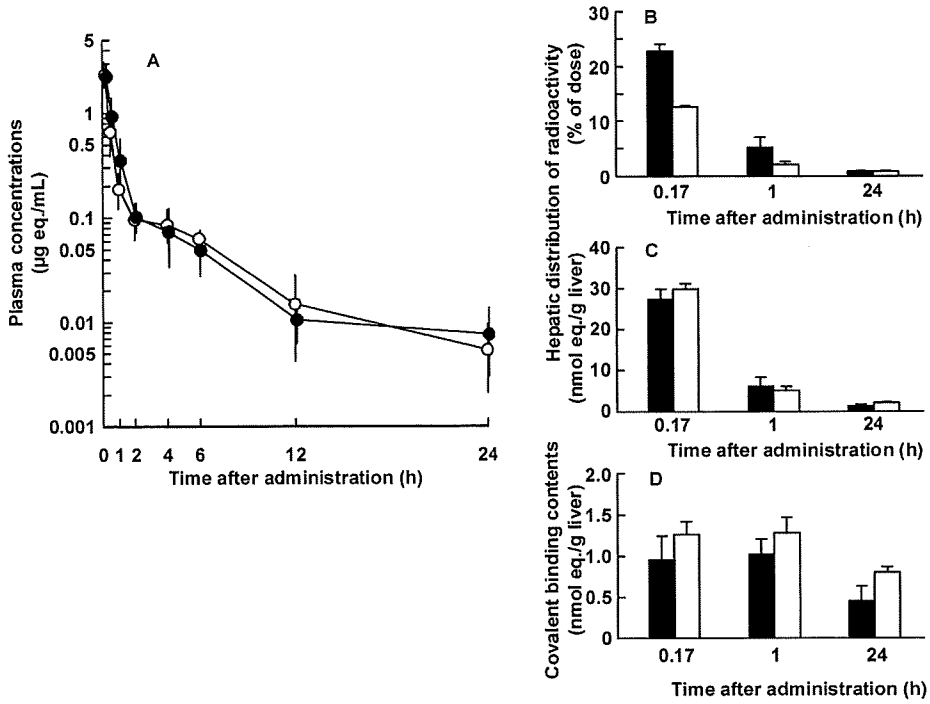

Figure 3. Plasma (A) or liver (B,C) concentrations of radiolabeled 5-*n*-butyl-pyrazolo[1,5-*a*]pyrimidine (M-5) and covalent protein binding to liver fractions (D) in chimeric mice with human (●, ■) or rat (○, □) livers after intravenous administration. ^{14}C-5-*n*-Butyl-pyrazolo[1,5-*a*]pyrimidine was administered intravenously at a dose of 3.0 mg/kg in the chimeric mice. Results are expressed as the mean values ± SD of three mice.

Table 1. Animal Profiles and Pharmacokinetic Parameters of Plasma Radioactivity Levels of Human- or Rat-Chimeric Mice after Intravenous Administration of 3.0 mg/kg of ^{14}C-5-*n*-Butyl-pyrazolo[1,5-*a*]pyrimidine (M-5)[a]

	chimeric mice with	
	human liver	rat liver
body weight (g)	20.9 ± 0.8	24.2 ± 1.7
liver weight (g)	2.27 ± 0.18	1.50 ± 0.14
extent of the replacement from mice to humans (%)	85.8 ± 7.0	
albumin concentrations in plasma (mg/mL)	8.43 ± 2.57	8.20 ± 2.43
C_0 (μg equiv/mL)	3.11 ± 0.44	3.52 ± 0.61
$AUC_{0\text{-}t}$ (μg equiv/mL·h)	2.11 ± 0.40	2.04 ± 0.28
$AUC_{0\text{-}\infty}$ (μg equiv/mL·h)	2.16 ± 0.41	2.06 ± 0.29
$t_{1/2}\alpha$ (h)	0.31 ± 0.06	0.23 ± 0.01
$t_{1/2}\beta$ (h)	6.17 ± 1.28	4.79 ± 0.26
CL_{tot} (L/h/kg)	1.42 ± 0.28	1.47 ± 0.22
Vd (L/kg)	0.98 ± 0.13	0.87 ± 0.17
MRT (h)	3.06 ± 0.64	2.98 ± 0.42
Vdss (L/kg)	4.40 ± 1.52	4.45 ± 1.28

[a] C_0, concentrations at time 0; $AUC_{0\text{-}t}$, areas under the plasma concentration−time curves from time 0 to the last detectable concentration; $AUC_{0\text{-}\infty}$, area under the plasma concentration−time curves from time 0 to the infinite time after administration; $t_{1/2}$, half-life; CL_{tot}, total systemic clearances; *Vd*, volume of distribution; *MRT*, mean residence times; *Vdss*, volume of distribution at steady state. See Experimental Procedures for details. Data are the means (±SD) from three mice.

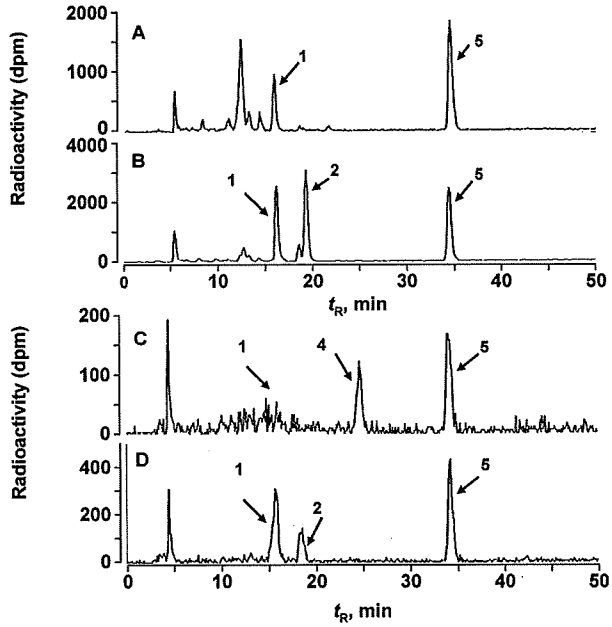

Figure 4. Representative radio-LC chromatograms of *in vivo* metabolites of radiolabeled 5-*n*-butyl-pyrazolo[1,5-*a*]pyrimidine (M-5) in plasma (A,B) and livers (C,D) at 10 min after intravenous administration to chimeric mice with human (A,C) or rat (B,D) livers. Peaks 1−5 shown here are the same as those described in the legend for Figure 2: peak 1, a glutathione conjugate of M-23OH; peak 2, a rat-specific unknown product; peak 4, M-23OH; and peak 5, 5-*n*-butyl-pyrazolo[1,5-*a*]pyrimidine (M-5).

M-23OH-glutathione conjugate was detected at almost the background level or a minor level in the liver (Figure 4C). On the contrary, chimeric mice with rat livers had the rat-specific metabolite peak corresponding to an unknown metabolite in the chromatograms obtained from the plasma and liver *in vivo* (Figure 4B,D), like the *in vitro* rat P450 1A2 system (Figure 2C,D).

Analysis of *in Vivo* Covalent Binding of 5-*n*-Butyl-pyrazolo[1,5-*a*]pyrimidine to Liver Microsomal or Cytosolic Proteins in Chimeric Mice with Human Livers. Covalent binding of 5-*n*-butyl-pyrazolo[1,5-*a*]pyrimidine in liver microsomal proteins from the chimeric mice with human livers after the administration of ^{14}C-5-*n*-butyl-pyrazolo[1,5-*a*]pyrimidine was analyzed first by SDS−PAGE. As shown in Figure 5A, many bands existed in the gel after Coomassie blue staining: 10 protein bands in the ranges of 35−100 kDa in the liver microsomes were focused. After measurements of protein contents (Figure 5B) and radioactivities (Figure 5C) of the 10 analyte pieces, specific covalent binding of 5-*n*-butyl-pyrazolo[1,5-*a*]pyrimidine

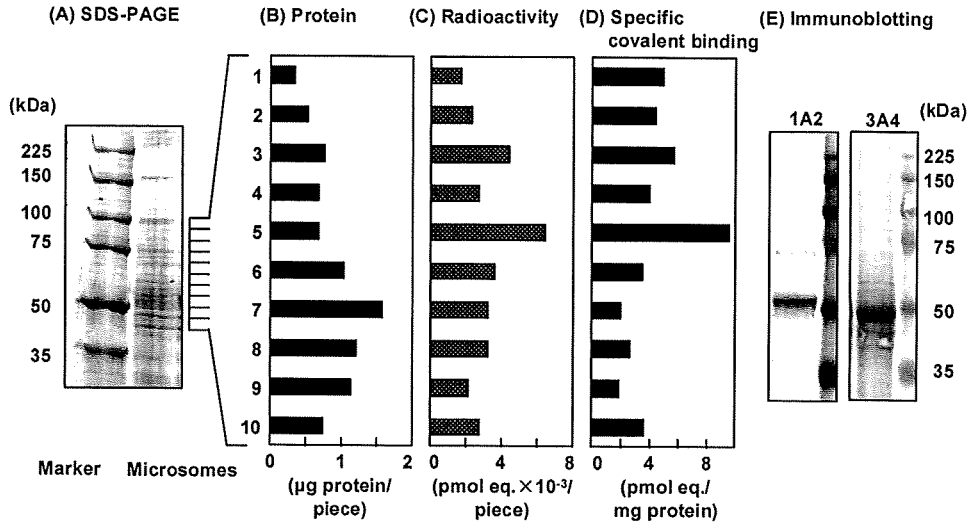

Figure 5. Covalent binding analysis after SDS−PAGE of liver microsomal proteins obtained from chimeric mice with humanized liver after the administration of radiolabeled 5-*n*-butyl-pyrazolo[1,5-*a*]pyrimidine (M-5). SDS−polyacrylamide gel electrophoretogram (A) was stained with Coomassie Brilliant Blue. Protein (B) and radioactivity (C) contents of each piece on the gel were determined. Specific covalent binding contents were expressed as pmol 5-*n*-butyl-pyrazolo[1,5-*a*]pyrimidine bound per mg microsomal protein (D).

was calculated (Figure 5D). Approximately 2−10 pmol equivalents of 5-*n*-butyl-pyrazolo[1,5-*a*]pyrimidine bound to a variety of liver microsomal proteins per mg total microsomal protein. The radioactivities from metabolically activated 5-*n*-butyl-pyrazolo[1,5-*a*]pyrimidine bound to human P450 1A2 (fraction 7, Figure 5E), P450 3A4 (fraction 8, Figure 5E), and other many microsomal proteins including P450 2C9, 2C19, and 2D6 in humanized livers were judged from immunoblotting and molecular weights on the gel.

Covalent binding profiles of liver microsomal and cytosolic fractions were further investigated by two-dimensional electrophoresis in the chimeric mice with humanized livers after the administration of radiolabeled 5-*n*-butyl-pyrazolo[1,5-*a*]pyrimidine. Protein samples (100 μg) were separated by isoelectric points (pH 3−10) and molecular weight (10−225 kDa) (Figure 6A,B). Protein contents and covalent binding contents of these analyte spots in the gels were determined. Two-dimensional electrophoresis associated with accelerator mass spectrometry analyses revealed that 5-*n*-butyl-pyrazolo[1,5-*a*]pyrimidine bound covalently to a variety of liver microsomal (Figure 6C) and cytosolic (Figure 6D) proteins. The highest specific binding was observed in prolyl-4-hydroxylase (0.016 pmol equiv/μg protein, a key enzyme in the biosynthesis of collagens) in microsomal proteins (a spot of 0.15 μg protein/mg microsomal protein shown in Figure 6C) and an antioxidant enzyme catalase (0.0099 pmol equiv/μg protein, a spot of 1.26 μg protein/mg cytosolic protein shown in Figure 6D) in cytosolic proteins, respectively, after two-dimensional electrophoresis and accelerator mass spectrometry analysis.

Discussion

Idiosyncratic drug toxicity like hepatotoxicity is a major complication of drug therapy and drug development. Many idiosyncratic reactions appear to have an immunological etiology with increasing evidence for the role of T-lymphocytes (*18*). Toxicity testing has been ineffective in the prediction of drug candidates that will be associated with a relatively high incidence of idiosyncratic drug reactions. Circumstantial evidence suggests the involvement of reactive metabolites in the etiology of these reactions, and this has prompted several companies to screen drug candidates for the formation of such compounds (*19*). It has been suggested that bioactivated small organic molecules *in vivo* resulting in electrophiles can adduct to biological macromolecules (approximately 1 nmol drug equiv/mg protein) and subsequently elicit organ toxicity (*20*). To reduce this figure by 20-fold gave a conservative target threshold value for *in vivo* covalent binding of 50 pmol drug equiv/mg protein (*20*). *In vitro* covalent binding analysis of drug candidates bioactivated by human liver microsomes is generally available for safety tests (*20*). To develop efficient prediction methods, a better understanding of the basic mechanisms involved is essential. Established chimeric mice with humanized livers (*7, 8*) would be good predictors compared with human liver microsomes because these livers have both microsomal and cytosolic enzyme systems for understanding whole drug metabolism and disposition *in vivo*. In our analysis for the evaluation of drug−protein adducts *in vivo*, a new approach by electrophoresis associated with accelerator mass spectrometry was first adapted. The low but measurable radioactivity in separated spots on the gel determined by accelerator mass spectrometry in this study could yield a new evaluation system for the drug-target proteins (as discussed below).

The present target compound 5-*n*-butyl-pyrazolo[1,5-*a*]pyrimidine (Figure 1) is the primary metabolite of a previous drug candidate, 5-*n*-butyl-7-(3,4,5-trimethoxybenzoylamino)pyrazolo[1,5-*a*]pyrimidine, with a potential analgesic effect (*5*). Bioactivation of this model compound was effectively catalyzed by recombinant human P450 1A2 (Figure 2) *in vitro* and also by livers in humanized mice *in vivo* through C^3-hydroxylation to form covalent protein binding (Figure 3) and a glutathione adduct (Figure 4). On the contrary, chimeric mice with rat livers had some rat-specific metabolites *in vivo* (Figure 4). These results demonstrated that livers of the chimeric mice with humanized livers could activate 5-*n*-butyl-pyrazolo[1,5-*a*]pyrimidine *in vivo*, leading to human-selective covalent binding and that the *in vivo* metabolic pattern of 5-*n*-butyl-pyrazolo[1,5-*a*]-pyrimidine was the same as that of *in vitro* metabolites in human liver microsomes (*5*) or recombinant human P450 1A2 shown here by radio-LC systems.

Profiles of the drug−protein adducts from bioactivated 5-*n*-butyl-pyrazolo[1,5-*a*]pyrimidine were analyzed by separations with SDS−PAGE (Figure 5) and two-dimensional electrophoresis (Figure 6). P450 1A2 in humanized liver was capable of oxidizing 5-*n*-butyl-pyrazolo[1,5-*a*]pyrimidine at the C^3-position

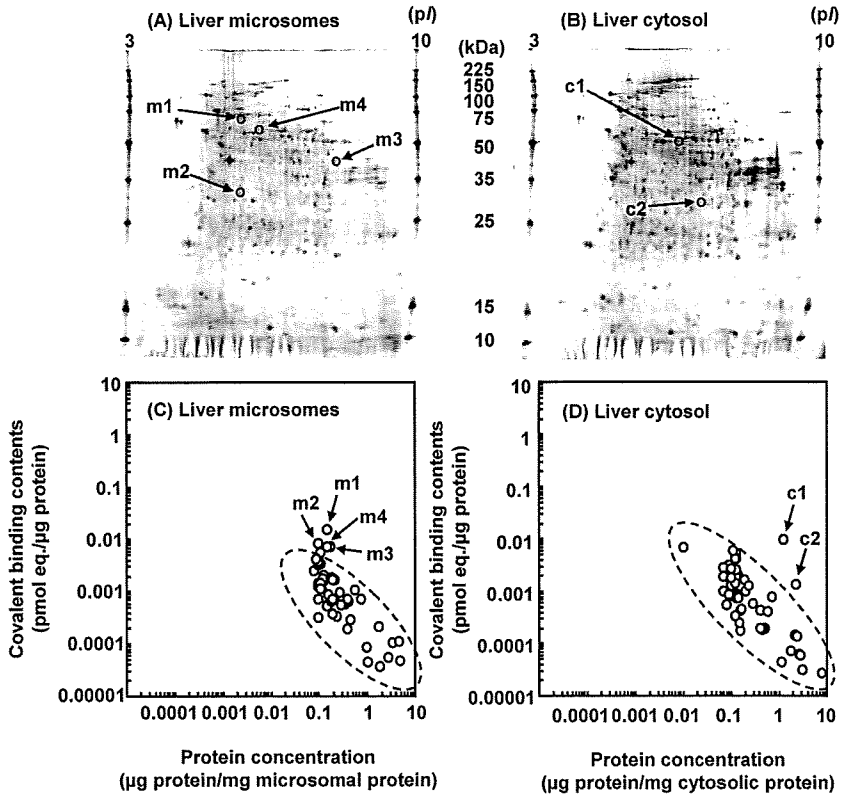

Figure 6. Covalent binding profiles of liver microsomal (A,C) and cytosolic (B,D) protein fractions separated by two-dimensional electrophoresis obtained from chimeric mice with humanized liver after the administration of radiolabeled 5-*n*-butyl-pyrazolo[1,5-*a*]pyrimidine (M-5). Loaded protein samples (100 μg) were focused (*x* axis, cathode on the right) and then separated by SDS−PAGE (*y* axis, dye front at bottom) with SYPRO Ruby staining (A,B). *In vivo* protein binding derived from metabolically activated ^{14}C-5-*n*-butyl-pyrazolo[1,5-*a*]pyrimidine was analyzed by accelerator mass spectrometry (C,D). The typical proteins shown with arrows are m1, prolyl-4-hydroxylase (NCBI accession number gi: 602675); m2, 3-hydroxyanthranic acid dioxygenase (gi: 443919); m3, branched-chain-amino-acid aminotransferase (gi: 2052346); m4, selenium binding protein 1 (acetaminophen binding protein, gi: 16306550); c1, catalase (gi: 4557014); and c2, glutathione *S*-transferase, GSTM2 (gi: 54696748).

to the bioactivated metabolite and was adducted by this to some extent (Figure 5D). The P450 1A2 was separated into fraction 7 in Figure 5B. This fraction 7 on the gel also had P450 2C9 and other proteins with the apparent specific binding of ~2 pmol equiv/mg protein. It would be speculated that the bioactivated 5-*n*-butyl-pyrazolo[1,5-*a*]pyrimidine by P450 1A2 in humanized liver might bind P450 1A2 itself extensively and other surrounding abundant P450 forms or any proteins nonselectively. These P450 forms were not evaluated in two-dimensional electrophoresis because of technical reasons: the membrane-bound proteins were generally difficult to resolve by the first pI-dependent separation step in two-dimensional electrophoresis. However, relatively high specific covalent binding (~2 pmol equiv/μg protein) in the 35−100 kDa proteins (Figure 5) was detected when compared with that of any spots separated in two-dimensional electrophoresis (Figure 6). The drug−protein adducts of bioactivated 5-*n*-butyl-pyrazolo[1,5-*a*]pyrimidine were likely to nonselectively bind any abundant proteins in microsomal or cytosolic proteins shown in Figure 6C and D. Estimated specific bindings (pmol drug equiv/μg protein) apparently indicated an inverse correlation with the protein contents. One of the identified adducted targets was microsomal prolyl-4-hydroxylase, a key enzyme in the biosynthesis of collagens, or an cytosolic antioxidant enzyme catalase that catalyzes the decomposition of hydrogen peroxide to water and oxygen. These lines of evidence strongly suggest that 5-*n*-butyl-pyrazolo[1,5-*a*]pyrimidine, the primary metabolite of a hepatotoxic previous drug candidate for humans, could be bioactivated by human P450 1A2 in humanized liver *in vivo* and would bind any proteins either in microsomes or cytosol including the catalysis of P450 1A2 itself. It could be proposed that covalent binding of drugs via reactive quinone-imine derivatives might show relatively low specificities in target protein bindings.

In conclusion, the hepatotoxic proximate compound 5-*n*-butyl-pyrazolo[1,5-*a*]pyrimidine was activated by human liver microsomal P450 1A2 to reactive intermediate(s) *in vivo* in humanized chimeric mice and could relatively nonspecifically bind to biomolecules such as P450 1A2 and others. Chimeric mice with a human or rat livers would be good predictors to see idiosyncratic drug toxicity *in vivo* in preclinical studies.

Acknowledgment. This work was supported in part by the Ministry of Education, Science, Sports and Culture of Japan. We thank Drs. Norie Murayama and Makiko Shimizu for their assistance.

References

(1) Guengerich, F. P. (2008) Cytochrome P450 and chemical toxicology. *Chem. Res. Toxicol. 21*, 70–83.
(2) James, L. P., Mayeux, P. R., and Hinson, J. A. (2003) Acetaminophen-induced hepatotoxicity. *Drug Metab. Dispos. 31*, 1499–1506.
(3) Kassahun, K., Pearson, P. G., Tang, W., McIntosh, I., Leung, K., Elmore, C., Dean, D., Wang, R., Doss, G., and Baillie, T. A. (2001) Studies on the metabolism of troglitazone to reactive intermediates in vitro and in vivo. Evidence for novel biotransformation pathways involving quinone methide formation and thiazolidinedione ring scission. *Chem. Res. Toxicol. 14*, 62–70.
(4) Gonzalez, F. J., and Yu, A. M. (2006) Cytochrome P450 and xenobiotic receptor humanized mice. *Annu. Rev. Pharmacol. Toxicol. 46*, 41–64.
(5) Kuribayashi, S., Goto, K., Naito, S., Kamataki, T., and Yamazaki, H. (2009) Human cytochrome P450 1A2 involvement in the formation of reactive metabolites from a species-specific hepatotoxic pyrazolopyrimidine derivative, 5-n-butyl-7-(3,4,5-trimethoxybenzoylamino)pyrazolo[1,5-*a*]pyrimidine. *Chem. Res. Toxicol. 22*, 323–331.

(6) Powley, M. W., Frederick, C. B., Sistare, F. D., and DeGeorge, J. J. (2009) Safety assessment of drug metabolites: implications of regulatory guidance and potential application of genetically engineered mouse models that express human P450s. *Chem. Res. Toxicol. 22*, 257–262.
(7) Tateno, C., Yoshizane, Y., Saito, N., Kataoka, M., Utoh, R., Yamasaki, C., Tachibana, A., Soeno, Y., Asahina, K., Hino, H., Asahara, T., Yokoi, T., Furukawa, T., and Yoshizato, K. (2004) Near completely humanized liver in mice shows human-type metabolic responses to drugs. *Am. J. Pathol. 165*, 901–912.
(8) Katoh, M., Tateno, C., Yoshizato, K., and Yokoi, T. (2008) Chimeric mice with humanized liver. *Toxicology 246*, 9–17.
(9) Emoto, K., Tateno, C., Hino, H., Amano, H., Imaoka, Y., Asahina, K., Asahara, T., and Yoshizato, K. (2005) Efficient *in vivo* xenogeneic retroviral vector-mediated gene transduction into human hepatocytes. *Hum. Gene Ther. 16*, 1168–1174.
(10) Inoue, T., Sugihara, K., Ohshita, H., Horie, T., Kitamura, S., and Ohta, S. (2009) Prediction of human disposition toward *S*-^{3}H-warfarin using chimeric mice with humanized liver. *Drug Metab. Pharmacokinet. 24*, 153–160.
(11) Laemmli, U. K. (1970) Cleavage of structural proteins during the assembly of the head of bacteriophage T4. *Nature 227*, 680–685.
(12) Sanchez, J. C., Rouge, V., Pisteur, M., Ravier, F., Tonella, L., Moosmayer, M., Wilkins, M. R., and Hochstrasser, D. F. (1997) Improved and simplified in-gel sample application using reswelling of dry immobilized pH gradients. *Electrophoresis 18*, 324–327.
(13) Rabilloud, T., Valette, C., and Lawrence, J. J. (1994) Sample application by in-gel rehydration improves the resolution of two-dimensional electrophoresis with immobilized pH gradients in the first dimension. *Electrophoresis 15*, 1552–1558.
(14) Lopez, M. F., Berggren, K., Chernokalskaya, E., Lazarev, A., Robinson, M., and Patton, W. F. (2000) A comparison of silver stain and SYPRO Ruby Protein Gel Stain with respect to protein detection in two-dimensional gels and identification by peptide mass profiling. *Electrophoresis 21*, 3673–3683.
(15) Kristensen, D. B., Imamura, K., Miyamoto, Y., and Yoshizato, K. (2000) Mass spectrometric approaches for the characterization of proteins on a hybrid quadrupole time-of-flight (Q-TOF) mass spectrometer. *Electrophoresis 21*, 430–439.
(16) Gharahdaghi, F., Weinberg, C. R., Meagher, D. A., Imai, B. S., and Mische, S. M. (1999) Mass spectrometric identification of proteins from silver-stained polyacrylamide gel: a method for the removal of silver ions to enhance sensitivity. *Electrophoresis 20*, 601–605.
(17) Miyaoka, T., Isono, Y., Setani, K., Sakai, K., Yamada, I., Sato, Y., Gunji, S., and Matsui, T. (2007) Bioanalysis works in the IAA AMS facility: Comparison of AMS analytical method with LSC method in human mass balance study. *Nucl. Instrum. Methods Phys. Res., Sect. B 259*, 779–785.
(18) Park, B. K., Kitteringham, N. R., Powell, H., and Pirmohamed, M. (2000) Advances in molecular toxicology-towards understanding idiosyncratic drug toxicity. *Toxicology 153*, 39–60.
(19) Uetrecht, J. (2003) Screening for the potential of a drug candidate to cause idiosyncratic drug reactions. *Drug Discovery Today 8*, 832–837.
(20) Evans, D. C., Watt, A. P., Nicoll-Griffith, D. A., and Baillie, T. A. (2004) Drug-protein adducts: An industry perspective on minimizing the potential for drug bioactivation in drug discovery and development. *Chem. Res. Toxicol. 17*, 3–16.

TX900323A